

This discussion paper is/has been under review for the journal *Atmospheric Chemistry and Physics (ACP)*. Please refer to the corresponding final paper in *ACP* if available.

**Primary and
secondary organic
carbon downwind of
Mexico City**

X.-Y. Yu et al.

Primary and secondary organic carbon downwind of Mexico City

X.-Y. Yu¹, R. A. Cary², and N. S. Laulainen¹

¹Pacific Northwest National Laboratory, Richland, WA 99352, USA

²Sunset Laboratory Inc., 10160 SW Nimbus Ave., Tigard, OR 97223, USA

Received: 7 October 2008 – Accepted: 4 November 2008 – Published: 8 January 2009

Correspondence to: X.-Y. Yu (xiaoying.yu@pnl.gov)

Published by Copernicus Publications on behalf of the European Geosciences Union.

Title Page

Abstract

Introduction

Conclusions

References

Tables

Figures

⏪

⏩

◀

▶

Back

Close

Full Screen / Esc

Printer-friendly Version

Interactive Discussion

Abstract

In order to study particulate matter transport and transformation in the Megacity environment, fine particulate carbons were measured simultaneously at two supersites, suburban T1 and rural T2, downwind of Mexico City during the MILAGRO field campaign in March 2006. Organic carbon (OC), element carbon (EC), and total carbon (TC=OC+EC) were determined in near real-time using a Sunset semi-continuous OC/EC field analyzer. The semi-empirical EC tracer method was used to derive primary organic carbon (POC) and secondary organic carbon (SOC). Diurnal variations of primary and secondary carbons were observed at T1 and T2, which resulted from boundary layer inversion and impacted by local traffic patterns. The majority of organic carbon particles at T1 and T2 were secondary. The SOC% ($\text{SOC}\% = \text{SOC}/\text{TC} \times 100\%$) at T1 ranged from 1.2–100% with an average of $80.7 \pm 14.4\%$. The SOC% at T2 ranged from 12.8–100% with an average of $80.1 \pm 14.0\%$. The average EC to $\text{PM}_{2.5}$ percentage ($\text{EC}_{\text{PM}}\% = \text{EC}/\text{PM}_{2.5} \times 100\%$) and $\text{OC}_{\text{PM}}\%$ were 6.0% and 20.0% over the whole sampling time at T1. The POC to PM percentage ($\text{POC}_{\text{PM}}\%$) and $\text{SOC}_{\text{PM}}\%$ were 3.7% and 16.3%, respectively at the same site. The maximum $\text{EC}_{\text{PM}}\%$ was 21.2%, and the maximum $\text{OC}_{\text{PM}}\%$ was 57.2% at T1. The maximum $\text{POC}_{\text{PM}}\%$ was 12.9%, and the maximum $\text{SOC}_{\text{PM}}\%$ was 49.7% at the suburban site. Comparison of SOC and POC at T1 and T2 showed similar characteristics under favorable meteorological conditions, which indicated that transport between the two supersites took place. Strong correlations between EC and carbon monoxide (CO) and odd nitrogen species (NO and NO_x) were observed at T1. This indicated that EC had nearby sources, such as local traffic emissions. The EC/CO ratio derived by linear regression analysis, when parameters in $\mu\text{g C}/\text{m}^3$ and $\mu\text{g}/\text{m}^3$, respectively, was 0.0045 at T1. Correlations were also seen between OC and SOC vs. the sum of oxidants, such as O_3 and NO_2 , suggesting the secondary nature of carbons observed at T1.

Primary and secondary organic carbon downwind of Mexico City

X.-Y. Yu et al.

Title Page

Abstract

Introduction

Conclusions

References

Tables

Figures

⏪

⏩

◀

▶

Back

Close

Full Screen / Esc

Printer-friendly Version

Interactive Discussion



1 Introduction

The Megacity Initiative: Local and Global Research Observations (MILAGRO) Campaign took place in Mexico City area and Veracruz in March 2006. It consisted of four simultaneous measurement campaigns, MCMA-2006 (The Mexico City Metropolitan Area – 2006 Experiment), MAX-Mex (The Megacity Aerosol Experiment), MIRAGE-Mex (Megacity Impacts on Regional and Global Environments), and INTEX-B (Intercontinental Chemical Transport Experiment – B); each had different objectives. The Pacific Northwest National Laboratory (PNNL) participated in the MAX-Mex and MIRAGE-Mex campaigns. Using Mexico City as the base of the field studies, as well as multiple platforms, the experiments focused on characterization of aerosol properties, formation, and transformation spatially in the outflow from the urban center. Three main ground sites, T0, T1, and T2, were selected to conduct the field campaign on the ground level. T0 was located at the Instituto Mexican del Petroleo at the city center. T1 was at the Universidad Tecnologica de Tecamac in Estado de Mexico, and T2 was at Rancho La Bisnaga near Tizayuca, Hidalgo.

This paper describes the characterization of particulate organic carbon (OC) and elemental carbon (EC) using the Sunset semi-continuous OCEC field analyzer at T1 and T2. Doran et al. (2007) reported on the evolution of aerosol optical properties derived from several particle measurements downwind of Mexico City. This paper differs from these recently published results (Doran et al., 2007), as its focus is on the chemical characteristics of carbon species at T1 and T2. Detailed analysis of primary organic carbon (POC) and secondary organic carbon (SOC) using the semi-empirical EC tracer method was summarized in this paper. Combined with meteorological findings (Fast et al., 2007; Shaw et al., 2007), we investigated potential emission sources of OC, EC, POC, and SOC at T1 and T2. Characteristics of carbons during T1 to T2 transport favorable and unfavorable days were studied. In addition, an effort was made to decipher the relationship between carbonaceous species such as OC, EC, POC, and SOC and other pollutants, including ozone (O_3), odd nitrogen species (NO_x , NO ,

ACPD

9, 541–593, 2009

Primary and secondary organic carbon downwind of Mexico City

X.-Y. Yu et al.

Title Page

Abstract

Introduction

Conclusions

References

Tables

Figures

⏪

⏩

◀

▶

Back

Close

Full Screen / Esc

Printer-friendly Version

Interactive Discussion

and NO₂), sulfur dioxide (SO₂), and carbon monoxide (CO).

2 Experimental

2.1 Field site description

One of the main science drivers in the MILAGRO field design was to investigate evolution of trace gases and particulate matter from anthropogenic sources in Mexico City and their transport and effects on local and regional air quality and climate forcing. Three surface super sites, T0, T1, and T2, in the metropolitan Mexico City area were chosen during the MILAGRO campaign. The main idea was to sample pollutants following the Lagrangian flow when meteorological conditions were favorable downwind of Mexico City. Their relative location to each other and to other simultaneous observation sites is illustrated in Fig. 1. The T0 site at the Instituto Mexicano De Petroleo (19.29°23.60 N, 99.0855.60 W, 2243 m) was situated northwest of the basin on the central Mexican plateau. The T0 site was selected to capture fresh pollutants from the Mexico City. The T1 site at the Tecamac University (19.703 N, 98.982 W, 2270 m) was about 50 km northeast from the T0 site. It was chosen to capture fresh and aged particle transported from T0 before leaving the metropolitan area. The T2 site at Rancho la Bisnaga (20.010 N, 98.906 W, 2542 m) was about 35 km northeast of T1 at a higher elevation. It was chosen to measure aged pollutants from the Mexico City, in a non-urban area (Doran et al., 2007; Fast et al., 2007). The PNNL team conducted measurements at two surface sites, T1 and T2, during the MILAGRO campaign. Continuous sampling started on 9 March 2006 and ended on 30 March 2006.

Primary and secondary organic carbon downwind of Mexico City

X.-Y. Yu et al.

Title Page

Abstract

Introduction

Conclusions

References

Tables

Figures

⏪

⏩

◀

▶

Back

Close

Full Screen / Esc

Printer-friendly Version

Interactive Discussion

2.2 Instrumentation

2.2.1 Aerosol sampling stacks and inlets

In order to eliminate interference from near ground activities, an aerosol sampling stack was used adjacent to the PNNL research trailer at the T1 and T2 sites, respectively.

5 The sampling stack was made of PVC pipe ~20 cm in diameter and extending ~8 m above ground. The stack inlet was protected by a rain cap. A heated stainless steel sampling intake tube (~5 cm in diameter) was coaxially positioned in the center of stack ~4 m below the top of the stack and extending through the lower end cap. The airflow through the aerosol sampling stack was ~1000 lpm, of which approximately
10 120 lpm was drawn into the heated tube. The tube was wrapped with heating tape and insulation and further encased in a PVC pipe. Electric power was applied to heat the sample line such that the relative humidity (RH) of the sample air was maintained at or below 40%. A sampling manifold containing four sampling ports was used to divide the sample flow into 4 streams of nominally 30 lpm per line. One of the ports was used
15 to supply the PNNL Sunset OCEC field analyzer. The other ports were used to supply other aerosol instruments.

2.2.2 Sunset OCEC field analyzers

Two semi-continuous Sunset OCEC analyzers (Model 3F, Sunset Laboratory Inc., Portland, OR) were used to measure OC and EC mass loadings at the T1 and T2 sites.
20 Ambient samples were collected continuously by drawing a sample flow of ~8 lpm. A cyclone was used upstream of the instruments to pass particles smaller than 2.5 μm. The airstream also passed through a denuder to remove any volatile organic compounds in the air. Sample flow rate was adjusted for the pressure difference between sea level and each of the sites to ensure accurate conversion of sample volume. During
25 automated semi-continuous sampling, particulate matter was deposited on a quartz filter. The quartz filter was normally installed with a second backup filter, mostly to serve

Primary and secondary organic carbon downwind of Mexico City

X.-Y. Yu et al.

Title Page

Abstract

Introduction

Conclusions

References

Tables

Figures

⏪

⏩

◀

▶

Back

Close

Full Screen / Esc

Printer-friendly Version

Interactive Discussion

as support for the front filter. The portion of the sample tube containing the quartz filter was positioned within the central part of an oven, whose temperature was controlled by an instrument control and data logging program installed on a laptop computer and interfaced with the OCEC instrument.

After a sample was collected, *in situ* analysis was conducted by using the modified NIOSH method 5040, i.e., thermal optical transmittance analysis, to quantify OC and EC. The oven was first purged with helium (He) after a sample was collected. The temperature inside the oven was ramped up in a step fashion to 870°C to thermally desorb the organic compounds. The pyrolysis products were converted to carbon dioxide (CO₂) by the redox reaction with manganese dioxide. The CO₂ was quantified using a self-contained non-dispersive infrared (NDIR) laser detection system. In order to quantify EC using the thermal method, a second temperature ramp was applied while purging the oven with a mixture containing oxygen (O₂) and helium. During this stage, the elemental carbon was oxidized and the resulting CO₂ was detected by the NDIR detection system. At the end of each analysis, a fixed volume of external standard containing methane (CH₄) was injected and thus a known carbon mass could be derived. The external calibration was used in each analysis to insure repeatable quantification. The modified NIOSH thermal-optical transmittance protocol used during MILAGRO is summarized in Table 1.

Errors induced by pyrolysis of OC are corrected by continuously monitoring the absorbance of a tunable diode laser beam ($\lambda=660$ nm) passing through the sample filter. When the laser absorbance reaches the background level before the initial temperature ramping, the split point between OC and EC can be determined. OC and EC determined in this manner are defined as Thermal OC and Thermal EC. Total carbon (TC) is the sum of Thermal OC and Thermal EC, $TC=Thermal\ OC+Thermal\ EC$, or $TC=OC+EC$. The Sunset OCEC analyzer also provides an optical measurement of EC by laser transmission, i.e. Optical EC. Optical OC can be derived by subtracting Optical EC from total carbon, $Optical\ OC=TC-Optical\ EC$, where TC is determined in the thermal analysis.

Primary and secondary organic carbon downwind of Mexico City

X.-Y. Yu et al.

Title Page

Abstract

Introduction

Conclusions

References

Tables

Figures

⏪

⏩

◀

▶

Back

Close

Full Screen / Esc

Printer-friendly Version

Interactive Discussion

**Primary and
secondary organic
carbon downwind of
Mexico City**X.-Y. Yu et al.

Filters were changed every few days before the laser correction factor reached 88%. Hourly sampling was conducted at both T1 and T2 sites, i.e., 45-min ambient sampling followed by 15 min thermal-optical analysis. Daily, at midnight, a 0-min sampling blank was taken. Both instruments were calibrated using an external filter with known OC and EC mass concentrations. External filters were also used to check the precision of the two instruments; the results of these tests were in excellent agreement. The relative standard deviations deduced from collocated in situ measurements between the two analyzers were 5.3%, 5.6%, 24.3%, and 9.6% for Thermal OC, Optical OC, Thermal EC, and Optical EC, respectively. Details of these experiments are reported elsewhere (Bauer et al., 2009). The limits of detection for OC and EC determined using the thermal-optical method were estimated to be approximately $0.2 \mu\text{g C}/\text{m}^2$ (Schauer et al., 2003). These values are consistent with subsequent tests with the two PNNL units after the MILAGRO campaign (Bauer et al., 2009).

Quantities directly determined using the thermal-optical protocol, namely Thermal OC and Thermal EC, are used in the following discussions. Thermal OC and thermal EC are usually referred to as OC and EC. Comparison between the thermally and optically determined observables showed good agreement at T1 and T2 during the MILAGRO campaign. Figure 2a depicts the scatter plots between Optical EC and Thermal EC at T1 and T2. Similarly, Fig. 2b depicts the scatter plots between Optical OC and Thermal OC at T1 and T2. Fitting parameter results using linear least-squares regression analysis are summarized in Table 2. Good linearity and consistency are observed for Optical EC and Thermal EC at T1, as well as Optical OC and Thermal OC at both sites. The higher scatter of Optical EC vs. Thermal EC at T2 results mostly from the much lower mass loading of elemental carbon at T2.

Results shown in this paper are produced using linear least-squares fit and Deming least-squares fit procedures. When dealing with regression analysis with two variables, Deming regression analysis is recommended (Cornbleet and Gochman, 1979; Martin, 2000). The latter is considered to represent data with higher accuracy than linear least-squares analysis, because it considers two variables instead of one. Linear least-

[Title Page](#)[Abstract](#)[Introduction](#)[Conclusions](#)[References](#)[Tables](#)[Figures](#)[⏪](#)[⏩](#)[◀](#)[▶](#)[Back](#)[Close](#)[Full Screen / Esc](#)[Printer-friendly Version](#)[Interactive Discussion](#)

squares regression tends to underestimate the slope when the error along the x-axis is not considered. Comparison between Deming regression analysis and linear least-squares analysis of the same data showed a difference less than 5% for key fitting parameters (Bauer et al., 2009). This is true when data have good linearity.

5 2.2.3 Meteorology measurements

The boundary layer height was determined by the 915 MHz radar wind profiler (RWP) operated by the Argonne National Laboratory (ANL). The boundary layer depth was determined by a lidar at night at T1. Only RWP measurements were available at T2. Details of instrument setup, data processing, and intercomparison are described elsewhere (Shaw et al., 2007). General meteorology measurements at T1 were provided by R. L. Coulter at ANL and meteorology data from T2 were provided by our group at PNNL.

2.2.4 Trace gas measurements

Trace gases measurements including carbon monoxide (CO), ozone (O₃), sulfur dioxide (SO₂), and nitrogen oxides including nitric oxide (NO), nitrogen dioxide (NO₂), and NO_x (NO_x=NO+NO₂) were provided by the research groups of L. G. Huey at the Georgia Institute of Technology and R. Cohen at the University of California, Berkeley. Details of instrument principles of operation and configuration are described elsewhere (Chen et al., 2005; Nunnermacker et al., 1998). Time used in all measurements was often expressed in either local standard time (LST) or coordinated universal time (UTC). The difference between LST and UTC is 6 h in this experiment, UTC-6 h=LST.

Primary and secondary organic carbon downwind of Mexico City

X.-Y. Yu et al.

Title Page

Abstract

Introduction

Conclusions

References

Tables

Figures

⏪

⏩

◀

▶

Back

Close

Full Screen / Esc

Printer-friendly Version

Interactive Discussion

3 Results and discussion

3.1 Overview of OC and EC at T1 and T2

Simultaneous measurements of OC and EC at T1 and T2 revealed that the carbon composition at these two sites was quite different. Figure 3 depicts hourly-averaged Thermal OC, Thermal EC, TC, Thermal EC:TC ratio, and boundary layer height at T1 and T2 during the entire campaign. The night period during the month of March in Mexico City is shaded in light blue. Error bars are standard deviations of each observable.

A distinctive diurnal pattern is observed for OC, EC, and TC at T1. OC arrived at the first maximum at 8 a.m. (LST) at T1. A second peak of OC occurred at 2 p.m. EC reached its first peak at 6 a.m. Then it reached its second maximum at much reduced amplitude between 8–11 p.m. TC peaked first at 6 a.m., then at 2 p.m. during the early afternoon rush hour. The ratio of EC to TC (EC/TC) reached the first daily peak at 6 a.m., the second peak occurred between 2–6 p.m., similar to the trend observed with EC. The background mass loading was approximately $\sim 1 \mu\text{g C}/\text{m}^3$ for EC, $\sim 5 \mu\text{g C}/\text{m}^3$ for OC, and $\sim 6 \mu\text{g C}/\text{m}^3$, respectively at T1.

The boundary layer height remained shallow at night and early morning until approximately 8:30 a.m. (LST). It then began to grow and reached its maximum of $\sim 3300 \text{ m}$ above ground between 4–5 p.m. Thus, it is not surprising to observe the pronounced growth of EC, OC, and consequently TC at T1 in the early morning before the boundary layer height started to increase. Since T1 was located near a busy local express way and chosen to be downwind of the center of Mexico City, it received both fresh local anthropogenic emissions, as well as transport from the city when the meteorological conditions were suitable. The daily EC peak at 6 a.m. was likely caused by local early morning traffic. The slightly delayed OC peak at 8 a.m. could be a result of processing of both fresh and aged particles. The boundary layer diluting effect on particle matter mass loadings was seen in EC, OC, and TC.

Unlike T1, EC, OC, TC, and EC/TC did not present as a distinctive diurnal pattern

Title Page

Abstract

Introduction

Conclusions

References

Tables

Figures

⏪

⏩

◀

▶

Back

Close

Full Screen / Esc

Printer-friendly Version

Interactive Discussion



**Primary and
secondary organic
carbon downwind of
Mexico City**X.-Y. Yu et al.

[Title Page](#)[Abstract](#)[Introduction](#)[Conclusions](#)[References](#)[Tables](#)[Figures](#)[⏪](#)[⏩](#)[◀](#)[▶](#)[Back](#)[Close](#)[Full Screen / Esc](#)[Printer-friendly Version](#)[Interactive Discussion](#)

at T2. The baseline of OC stayed at $\sim 4 \mu\text{g C}/\text{m}^3$ and the baseline of EC stayed at $\sim 0.4 \mu\text{g C}/\text{m}^3$ at T2. The OC mass loading started to grow at 8 a.m. almost simultaneously as the boundary layer started to grow deeper. The OC first peaked at T2 between 9 and 10 a.m. (LST), it then reached its second maximum between 2–4 p.m. The growing boundary layer had the dilution effect which could explain partially why a higher mass loading peak was not observed later in the day at T2. A third OC peak occurred at midnight. The first daytime OC maximum at T2 was about two hours later than seen at T1. The same applied to the second daytime OC peak. Although EC massing loadings generally remained much lower at T2 than at T1, it peaked at 5 a.m. (LST), 7 a.m., 11 a.m., and 4 p.m. during day time. Two local maxima occurred at night at 7 p.m. and 11 p.m. after sunset. The TC reached its first maximum after sunrise between 9 and 10 a.m., its second peak between 3 and 5 p.m., and its third peak at midnight. The EC/TC peaked at 7 a.m. after sunrise, then twice at 11 a.m. and 4 p.m. After sunset, EC/TC peaked at 7 p.m. and 11 p.m. The EC/TC dipped at midnight, this was largely due to the local maximum of TC and the flat EC at the same hour. Since T2 was at a ranch in the middle of a hill far removed from busy interstate express ways and local traffic, it seemed that it was less affected by local anthropogenic emissions compared with T1 implied by the less pronounced diurnal pattern at T2.

3.2 Particulate OC and EC time series at T1 and T2

Time series of OC and EC at T1 and T2 are depicted in Fig. 4. Significant reduction of mass loadings was observed starting on 24 March 2006, when rain started at both sites. The rainy weather continued for the rest of the campaign. The last week of rain in fact formed a nice contrast with observations from the beginning of the campaign, when dry and warm weather persisted in the area. The time series of EC/TC from both sites are plotted in Fig. 5a. Statistics of mass loadings of EC, OC and TC, as well as EC/TC at T1 and T2 are summarized in Table 3. These results at T1 are comparable with measurements obtained by another Sunset OCEC analyzer located at the same

site (Stone et al., 2008). The statistics of OC and EC measurements for two weeks in March 2006 was reported in the latter. Significantly higher EC was observed at T1 than at T2. Although the average mass loadings of OC were fairly comparable between T1 and T2, the dynamic range was much wider at T1 than T2. The OC peaked at 29.3 $\mu\text{g C}/\text{m}^3$ on 22 March 2006; and the minimum value of 1.1 $\mu\text{g C}/\text{m}^3$ occurred on 23 March 2006 at T1. The highest OC occurred on 10 March, 2006; and the lowest on 24 March 2006 at T2.

3.3 The OC to EC ratios at T1 and T2

Another approach to evaluate OC and EC data was to look at the ratio of OC to EC (OC/EC) which gave indication of secondary and primary organic carbon at specific locations (Lim and Turpin, 2002; Turpin and Huntzicker, 1991; Turpin et al., 1991). The time series of OC/EC is shown in Fig. 5b. The data points are colored as a function of TC mass loadings at each site. The majority of OC/EC values at T1 are in the range of 1–10, with TC in the range of 1.2–40.5 $\mu\text{g C}/\text{m}^3$. On the other hand, OC/EC values at T2 are mostly in the range of 5–50, with TC in the range of 1.0–16.7 $\mu\text{g C}/\text{m}^3$. The EC/TC sometimes is used as an indicator of primary vs. secondary organic aerosols. The higher OC/EC values at T2 than T1 seem to imply that more processed particles are observed at T2 than at T1.

Figure 6a shows the scatter plots of OC vs. EC at T1 and T2. The data points are colored as a function of time during the month-long study. The solid lines are Deming fits. Results by linear least-squares regression and Deming regression analysis are summarized in Table 4. Much scatter of the data is seen in the scatter plot for OC vs. EC. This indicates that data at both sites could not be analyzed by a simple global linear regression analysis. Nonetheless, the global fit results in the OC/EC value from the fitting slope, which indicated that both primary and secondary organic carbons were observed at T1 and T2. When the same data were analyzed on daily basis (LST used to determine start and end points), very little correlation was found between OC and EC (see supplemental materials for details: <http://www.atmos-chem-phys-discuss.net/9/>)

Primary and secondary organic carbon downwind of Mexico City

X.-Y. Yu et al.

Title Page

Abstract

Introduction

Conclusions

References

Tables

Figures



Back

Close

Full Screen / Esc

Printer-friendly Version

Interactive Discussion



541/2009/acpd-9-541-2009-supplement.pdf). This further indicates the complexity of the OC and EC observed at both sites. When looking at the same data from a different perspective, e.g., as a function of OC/EC, as shown in Fig. 6b, the trend of the data becomes more obvious. The majority of the data points had OC/EC in the range of 0 to 10 at T1, while the majority of the data points at T2 had OC/EC in the range of 0 to 50. The difference in the OC/EC values indicates that the particles at T1 and T2 are of different character.

Table 5 shows a comparison of $PM_{2.5}$ OC and EC with other big cities in the world, such as Beijing, Shanghai, Hong Kong, Los Angeles, and Houston. Most of these OC and EC measurements were obtained by thermal optical reflectance methods (Birch, 1998; Cachier et al., 1989; Chow et al., 2001). Since the definitions of OC and EC are operationally defined, uncertainties exist among different methods. The OC/EC values for T1 and T2 reported in Table 5 are obtained by Deming regression analysis shown in Fig. 6a. The OC/EC value obtained at T1 is comparable to the average reported for urban US cities (Schichtel et al., 2008). In contrast, the average OC/EC value at T2 is comparable to places such as Houston (Russell and Allen, 2004) and Milan (Lonati et al., 2007). It is close to the average reported for US rural areas (Schichtel et al., 2008).

Although the averaged OC and EC at T1 and T2 in the vicinity of Mexico City did not rank the highest in this comparison, one needs to take into account that some of the other measurements were taken in different seasons, i.e., summer, fall, or winter. For example, winter observations usually result in higher mass loadings than those in summer. A better comparison is from Mexico City study in March 1997 (Chow et al., 2002). Six core sites were used in this study, La Merced, Pedregal, Xalostoc, Tlalnepantla, Netzahualcoyotl, and Cerro de la Estrella, mostly representing urban, suburban, residential, industrial, and commercial areas in or near downtown Mexico City. Results reported were averages of all six sites. The T1 and T2 comparisons with these results are in reasonable agreement. However, direct comparison with results from the regional sites may be more useful in illustrating changes or trends over the past decade. Unfortunately, the latter were not available. Querol et al. recently reported

**Primary and
secondary organic
carbon downwind of
Mexico City**X.-Y. Yu et al.

Title Page

Abstract

Introduction

Conclusions

References

Tables

Figures

⏪

⏩

◀

▶

Back

Close

Full Screen / Esc

Printer-friendly Version

Interactive Discussion

the OC and EC results during MILAGRO (Querol et al., 2008), but only results from T1 were available for comparison. Both their results of OC and EC were lower than our findings, but TC was higher. Since Querol et al. (2008) selected only a few 6 h samples to determine OC and EC, their results do not have the same time resolution or as many samples as reported here. We expect, therefore, that our results may provide more reliable statistics because of the continuous hourly measurements.

3.4 The semi-empirical EC tracer method

Although the OC/EC and EC/TC could be used to get some idea of the extent of primary and secondary organic carbon, quantification of POC and SOC is still needed. Identification of POC and SOC is quite important in further analysis. The semi-empirical EC tracer method is used here to derive POC and SOC empirically. The assumptions and methodology of EC tracer method are described in detail elsewhere (Castro et al., 1999; Turpin and Huntzicker, 1991; 1995; Yu et al., 2007). Briefly, total OC (OC_{total}) is defined as the sum of POC and SOC, Eq. (1).

$$SOC = OC_{total} - POC \quad (1)$$

POC is defined in Eq. (2),

$$POC = EC \times \left(\frac{OC}{EC} \right)_{pri} \quad (2)$$

where $(OC/EC)_{pri}$ is the estimated primary carbon ratio. The OC emitted from non-combustion sources, such as emission directly from vegetation, is assumed to be negligible in the approach used here. Using the minimum OC to EC ratio, $(OC/EC)_{min}$, to substitute for $(OC/EC)_{pri}$, the SOC and POC can therefore be estimated (Castro et al., 1999):

$$SOC = OC_{total} - EC \times \left(\frac{OC}{EC} \right)_{min} \quad (3)$$

Primary and secondary organic carbon downwind of Mexico City

X.-Y. Yu et al.

Title Page

Abstract

Introduction

Conclusions

References

Tables

Figures

◀

▶

◀

▶

Back

Close

Full Screen / Esc

Printer-friendly Version

Interactive Discussion



**Primary and
secondary organic
carbon downwind of
Mexico City**X.-Y. Yu et al.

Several assumptions must be made to deduce SOC and POC in this manner. For instance, samples used to calculate $(OC/EC)_{\min}$ have negligible amounts of SOC. Composition and emission sources of POC and SOC are assumed to be relatively constant spatially and temporally. Contribution from non-combustion POC is low. Contribution from semi-volatile organic compounds is also assumed to be low compared with non-volatile organic species. The determination of $(OC/EC)_{\min}$ is crucial in this approach.

Several methods are commonly used to derive SOC and POC, including the organic tracer-based receptor model (Schauer et al., 1996, 2002), the reactive chemical transport model (Pandis et al., 1992; Strader et al., 1999), the non-reactive transport model (Hildemann et al., 1996) and the semi-empirical EC tracer method (Castro et al., 1999; Turpin and Huntzicker, 1995). The EC tracer method is mainly dependent on ambient measurements of OC and EC and therefore is easy to use. The key is to estimate $(OC/EC)_{\text{pri}}$ from ambient conditions. The challenge lies because $(OC/EC)_{\text{pri}}$ could be influenced by meteorological conditions and emission fluctuations (Turpin and Huntzicker, 1995; Yu et al., 2004b). Recently several groups evaluated linear regression techniques, such as linear least-squares, Deming regression, and York regression, which are often used in the EC tracer method to derive secondary and primary organic carbon (Chu, 2005; Saylor et al., 2006).

Results from newer measurement techniques such as the Aerodyne Aerosol Mass Spectrometer (AMS) (Kondo et al., 2007; Takegawa et al., 2006) and the Particle-Into-Liquid Sampler coupled with Total Organic Carbon analyzer (PILS-TOC) were also used to derive secondary organic aerosols (Sullivan et al., 2006). The approach Takegawa et al. took to analyze the AMS data is conceptually similar to the semi-empirical EC tracer method; whereas secondary organic aerosol (SOA) formation was deferred from direct measurements of water-soluble organic carbon (WSOC) by PILS-TOC. The above two techniques provide an approximation of SOA. Comparison of SOA derived by different techniques will be of prime interest when these results in the form of time series become available.

[Title Page](#)[Abstract](#)[Introduction](#)[Conclusions](#)[References](#)[Tables](#)[Figures](#)[⏪](#)[⏩](#)[◀](#)[▶](#)[Back](#)[Close](#)[Full Screen / Esc](#)[Printer-friendly Version](#)[Interactive Discussion](#)

**Primary and
secondary organic
carbon downwind of
Mexico City**X.-Y. Yu et al.

[Title Page](#)[Abstract](#)[Introduction](#)[Conclusions](#)[References](#)[Tables](#)[Figures](#)[⏪](#)[⏩](#)[◀](#)[▶](#)[Back](#)[Close](#)[Full Screen / Esc](#)[Printer-friendly Version](#)[Interactive Discussion](#)

Previous authors often used the lowest 5% or 10% measured OC/EC values in a given season to estimate $(OC/EC)_{\min}$ (Lim and Turpin, 2002; Yuan et al., 2006). Table 6 summarizes the linear least-squares fit results of OC vs. EC from different subsets of the data from the lowest 2.5%, 5%, and 10% OC/EC values to estimate $(OC/EC)_{\text{pri}}$. For instance, the $(OC/EC)_{\text{pri}}$ at T1 is estimated to be 0.64 using the lowest 5% of OC/EC values by linear regression analysis. It is worth mentioning that Yuan et al. found that $(OC/EC)_{\text{pri}}$ is season-dependent. For instance, the $(OC/EC)_{\text{pri}}$ ranged from 0.41 to 0.88 from summer to winter based on observations in Hong Kong (Yuan et al., 2006). Therefore, the $(OC/EC)_{\text{pri}}$ determined in this particular study could not be used in all seasons for a similar site in Mexico City.

In addition, a second approach is used to obtain $(OC/EC)_{\text{pri}}$, since the R^2 values from the lowest 5% OC/EC approach are not as satisfactory. Table 7 summarizes the linear least-squares fit results of OC vs. EC grouped by binning OC/EC values in different ranges at each site. The $(OC/EC)_{\min}=0.61$ at T1 falls in the range of OC/EC values typical of fossil fuel sources. The R^2 value obtained is 0.95. On the other hand, $(OC/EC)_{\min}$ is 2.26 with the $R^2=0.86$ at T2. This value falls in the range of OC/EC values typical of biomass emissions (Gelencser et al., 2007). The results from this approach are in reasonable agreement with those using the lowest 2.5% or 5% of OC/EC data shown in Table 6. Since the results obtained by binning the OC and EC values to different ranges prior to applying linear least-squares analysis yields improved R^2 (Tables 6 and 7), the slopes from this regression analysis are used as $(OC/EC)_{\min}=(OC/EC)_{\text{pri}}$ to derive SOC and POC at T1 and T2.

3.5 SOC and POC at T1 and T2

Figure 7a and b shows the time series of OC, EC, SOC, POC, SOC%, wind direction, and wind speed at T1 and T2, respectively. The SOC% is defined as $SOC\%=SOC/OC\times 100\%$. In addition, the entire sampling period was categorized into three types of conditions: transport likely (shaded in gray), transport unlikely (shaded in

**Primary and
secondary organic
carbon downwind of
Mexico City**

X.-Y. Yu et al.

[Title Page](#)[Abstract](#)[Introduction](#)[Conclusions](#)[References](#)[Tables](#)[Figures](#)[⏪](#)[⏩](#)[◀](#)[▶](#)[Back](#)[Close](#)[Full Screen / Esc](#)[Printer-friendly Version](#)[Interactive Discussion](#)

blue), and transport possible (shaded in green), based on meteorological conditions favoring transport between T1 and T2 downwind of Mexico City (Fast et al., 2007). Likely transport dates are 9 March–12 March, 18 March–22 March, 24 March–25 March, and 30 March 2006. Possible transport dates are 8 March, 17 March, 23 March, and 26 March–29 March 2006. Unlikely transport dates are 13 March–16 March 2006. During likely transport days, the wind direction is south-westerly or westerly. The wind direction during possible transport days is southerly or westerly. The wind direction during unlikely transport days is predominantly southerly.

The SOC% at T1 ranged from 1.2–100% with an average of $80.7 \pm 14.4\%$. The SOC% at T2 ranged from 12.8–100% with an average of $80.1 \pm 14.0\%$. The SOC% values observed in Mexico City suburban and rural areas are close to what is observed in other locations with high secondary organic carbon, such as up to 80% in Southern California (Turpin and Huntzicker, 1995), 63–76% in Europe (Gelencser et al., 2007), 50–95% in Beijing (Dan et al., 2004), 84% in Milan (Lonati et al., 2007), and 78% on the Portuguese coast (Castro et al., 1999).

Figure 8 shows wind roses of SOC and POC at T1 and T2. Predominant wind directions at T1 were southerly, north-easterly, south-westerly, and westerly. Predominant wind directions at T2 were southerly, north-westerly, south-westerly, and westerly. The favorable transport conditions downwind of Mexico City mostly were from the south-west and west (Fast et al., 2007). The OC and EC observed at T1 and T2 were strongly influenced by the meteorological conditions. Since only hourly data were used in this analysis, they may not reflect the dynamics of rapid wind changes at the surface. However, this analysis does seem to provide a good idea of the effect of meteorological conditions on particulate matter mass loadings.

Emissions downwind of Mexico City or T0 were anticipated and observed, namely from the south and southwest. However, emissions from other directions, e.g., from the northwest and northeast, were higher than anticipated. The Tula-Vita-Asasco industrial corridor is 60 km north-north-west from the center of Mexico City. For instance, there is a large refinery and a power plant in Tula. Emissions from industrial sources from the

**Primary and
secondary organic
carbon downwind of
Mexico City**X.-Y. Yu et al.

[Title Page](#)[Abstract](#)[Introduction](#)[Conclusions](#)[References](#)[Tables](#)[Figures](#)[⏪](#)[⏩](#)[◀](#)[▶](#)[Back](#)[Close](#)[Full Screen / Esc](#)[Printer-friendly Version](#)[Interactive Discussion](#)

north and northwest, such as just mentioned, may have contributed to the POC and SOC observed at T1. Emissions from the southeast may come from the active volcano, Popocatepetl, 70 km southeast of the Mexico City, and Puebla, 129 km southeast of the Mexico City. Emissions from the northeast may come from Pachuca, an area with fast growing small and mid-sized industries. Similarly, emissions downwind of Mexico City from the south and southwest were observed at T2. A striking feature of the POC and SOC observed at T2 was the strong influence from northwest. It is likely that contributions of emissions from the Tula-Vita-Aspasco industrial areas exerted a stronger effect at T2 than T1.

Figure 9 depicts scatter plots of SOC vs. TC and POC vs. TC during the three T1 to T2 transport scenarios – likely, possible and unlikely. The solid lines are linear least-squares fits. During T1 to T2 favorable transport dates, i.e., likely and possible dates, the slopes generated by SOC vs. TC regression analysis were very similar between T1 and T2. However, this was not true with the T1 to T2 unlikely transport days. Similarly, the slopes generated by POC vs. TC regression analysis were almost identical during T1 to T2 likely and possible transport days, whereas the same was not true for unlikely transport days. This analysis indicates that we observed different patterns in the SOC and POC due to transport between T1 and T2 driven by meteorological conditions.

3.6 Weekday and weekend patterns

Diurnal variations of carbon concentrations at T1 and T2 during weekdays and weekends over the duration of the campaign are shown in Fig. 10. As discussed earlier, diurnal patterns of OC and EC were observed at T1 and T2. This could be a result of not only boundary layer dilution, but also traffic emissions during weekdays and weekends. General features of daily maxima of OC, EC, and TC are shown in Fig. 3. We now focus on the difference between weekday and weekend patterns. The OC/EC and SOC/POC values are in a similar range during the weekdays and the weekend at T1. On the other hand, OC/EC values at T2 are slightly higher during the weekdays than the weekends.

**Primary and
secondary organic
carbon downwind of
Mexico City**X.-Y. Yu et al.

[Title Page](#)[Abstract](#)[Introduction](#)[Conclusions](#)[References](#)[Tables](#)[Figures](#)[Back](#)[Close](#)[Full Screen / Esc](#)[Printer-friendly Version](#)[Interactive Discussion](#)

There are some major differences in the OC, EC, SOC and POC patterns between weekdays and weekends at T1. The EC has two pronounced peaks between 5–10 a.m. (LST) and 8 p.m.–2 a.m. during the weekend, whereas the EC has one major peak between 5–10 a.m. during weekdays. This bimodal behavior of EC could be caused by increasing vehicle emissions in the latter part of the day in the weekends. The OC has two peaks during the weekdays at T1. The first occurs between 5 to 10 a.m., and the second between noon to 6 p.m. The OC shares some similar features over the weekend. However, the magnitude of OC mass loadings is slightly higher between 5 to 10 a.m. in the weekend compared with the same time frame in the weekdays. The magnitude of OC mass loadings is slightly lower in the afternoon rush hours during the weekend compared with weekdays. In addition, a third OC peak occurs in the evening starting at 8 p.m. and ending at 2 a.m. in the morning during the weekend. In contrast, the OC mass loadings remain fairly constant at the same time in the weekdays. These observed features indicate that different traffic patterns can have an influence on the OC and EC mass loadings between weekdays and weekends.

The OC/EC and SOC/POC values are in a similar range during weekdays and the weekend at T2. The major difference of the OC and EC patterns between weekdays and weekends at T2 is that the OC and EC peaks are slightly delayed after sunrise during the weekend. For instance, the first EC peak after sunrise occurs at 7 a.m. during weekdays, whereas it occurs at 8–10 a.m. during the weekends. Similarly, the OC maximum occurs between noon and 4 p.m. during the weekdays, whereas it delays to 2–6 p.m. during the weekend. Peaks of OC and EC were often observed during morning and late afternoon rush hours (Allen et al., 1999; Chow et al., 2006; Jeong et al., 2004; Lim and Turpin, 2002; Plaza et al., 2006; Salma et al., 2004). Diurnal variations of SOC have been observed elsewhere (Harley et al., 2005; Strader et al., 1999). SOC formation could increase OC/EC values, while other sources could also complicate the determination of the stable primary emission ratio (Harley et al., 2005). It is known that the afternoon OC increase could be attributed to a combination of photochemical conversion of urban pollutants and boundary layer convection followed by

vertical and horizontal transport to non-urban locations. These observations indicate that differences in traffic patterns between weekdays and weekends at the suburban and rural sites may have affected the daily variations of carbon in addition to meteorological conditions (Watson and Chow, 2002).

5 A chemical mass balance model (CMB) based on molecular marker species was used to determine the relative contribution of major sources to ambient OC at T0 and T1 (Stone et al., 2008). CMB uses a set of molecular markers to apportion source contributions to ambient PM (Schauer et al., 1996). Model outputs usually include
10 relative contribution of vegetative detritus, diesel engines, gasoline vehicles, smoking vehicles, representative wood smokes, and non-apportioned or other sources of ambient OC. Motor vehicles were found to contribute 32% of ambient OC at T1 by Stone et al. T1 was also found to be influenced by local aerosol sources than urban outflow. Our observations and conclusions are in good agreement with these findings at T1.

3.7 EC, POC, and SOC emissions

15 Figure 11 shows the time series of hourly averaged NO, NO₂, SO₂, O₃, CO, OC, EC, PM_{2.5}, temperature, and RH at T1. The average EC to PM_{2.5} percentage ($EC_{PM}\% = EC/PM_{2.5} \times 100\%$) and $OC_{PM}\%$ were 6.0% and 20.0% over the entire sampling time at T1. The average POC to PM percentage ($POC_{PM}\%$) and $SOC_{PM}\%$ were 3.7% and 16.3%, respectively. The maximum $EC_{PM}\%$ was 21.2% and the maximum
20 $OC_{PM}\%$ was 57.2%. The maximum $POC_{PM}\%$ was 12.9% and the maximum $SOC_{PM}\%$ was 49.7%. These findings are similar to observations in big cities such as Beijing, Hong Kong, or Los Angeles (Duan et al., 2005; Turpin et al., 1991; Yu et al., 2004a).

Since trace gases such as CO, NO, NO₂, NO_x, O₃, and SO₂ play an important role in particulate formation and transformation, examining the relationship between EC, OC (POC and SOC) vs. trace gas species could provide more information on emissions sources (Chen et al., 2001). Scatter plots of EC vs. CO, EC vs. NO, and EC vs. NO_x (NO_x=NO+NO₂) of observations at T1 show reasonable correlations (Fig. 12a), which indicate that EC had nearby sources, such as traffic emissions, at the T1 site. Scat-

Primary and secondary organic carbon downwind of Mexico City

X.-Y. Yu et al.

Title Page

Abstract

Introduction

Conclusions

References

Tables

Figures



Back

Close

Full Screen / Esc

Printer-friendly Version

Interactive Discussion

ter plots of EC vs. SO₂ and EC vs. O₃ did not provide any strong correlations. Since SO₂ and O₃ were likely involved in secondary particle formation, this result is not surprising. Please refer to supplemental materials (<http://www.atmos-chem-phys-discuss.net/9/541/2009/acpd-9-541-2009-supplement.pdf>) for all figures mentioned for EC and

5 OC vs. trace gas species.

Since NO is a primary pollutant emitted from combustion processes, its correlation with EC confirms the primary nature of the EC fraction. Carbon monoxide is produced via incomplete combustion processes, mainly via motor vehicles exhaust in urban areas. It is often highly correlated with EC emissions (Chen et al., 2001; Park et al., 2005a; Wang et al., 2004). The EC to CO ratio (EC/CO) derived by linear regression analysis can be used to differentiate sources of air masses and estimate EC or CO emissions when direct measurements are not available. The EC/CO at T1 is determined to be 0.0045, for EC in µgC/m³ and CO in µg/m³, respectively. This result is similar to what was observed at the Baltimore supersite in the summer (Park et al., 2005b). Since the EC/CO value depends on multiple factors, further study could reveal more information about the difference of air masses and seasonal variations compared with other locations.

Similarly, scatter plots of OC vs. CO, OC vs. NO, OC vs. NO₂, OC vs. NO_x, OC vs. SO₂, or OC vs. O₃ do not show obvious correlations. However, stronger correlation is apparent when OC is plotted vs. the sum of oxidants NO₂ and O₃, or odd oxygen, O_x (Fig. 12b). This is because the sum of the oxidants better represents the degree of photochemical air pollution than NO₂ or O₃ alone. Correlation analysis suggests a predominantly secondary nature of OC at T1 during the campaign. This finding concurs with recent work conducted at a mountain top site within the Mexico City metropolitan area (Herndon et al., 2008). Although the individual scatter plots of SOC vs. O₃ and SOC vs. NO₂ do not reveal strong correlations (Fig. 13), SOC vs. O_x, or O₃+NO₂, shows improved correlations (Fig. 12b), further confirming the contribution of secondary organic carbon at T1. When POC and SOC are plotted separately against each of the trace gas species, a better trend is seen in some cases (see Fig. 13). For

**Primary and
secondary organic
carbon downwind of
Mexico City**

X.-Y. Yu et al.

Title Page

Abstract

Introduction

Conclusions

References

Tables

Figures



Back

Close

Full Screen / Esc

Printer-friendly Version

Interactive Discussion

instance, correlations between POC and CO, NO, or NO_x show good linearity, indicating that primary combustion-generated carbon emissions are important sources at T1 (Plaza et al., 2006). This also confirms that the estimates of POC and SOC using the EC tracer technique are reasonable.

5 The ISORROPIA-II thermodynamic equilibrium model was used to assess the contribution of SOA to the increase of WSOC concentrations at T1. This analysis focuses only on three days, 27 March 2006–29 March 2006 (Hennigan et al., 2008). The box model results indicate that secondary aerosol production is responsible for the increase of WSOC. SOA is concluded to be resulted from OH initiated photochemical reactions
10 from anthropogenic sources. Our results support the previous findings. Comparison with POC and SOC determined using other methodology will be useful to estimate uncertainties in each method in the future. Evaluation of contributions of the ozone and radical channels to organic aerosol formation is also of interest in future studies.

4 Conclusions

15 Elemental carbon and organic carbon were measured near real-time by the Sunset semi-continuous OCEC field analyzer at T1 and T2 during the MILAGRO field study. High carbonaceous mass loadings were observed in the vicinity and downwind of Mexico City. Higher OC and EC were observed at T1 than at T2. The EC at T2 were particularly low, whereas T1 saw more fresh emissions from possibly the nearby highways and local traffic. Diurnal variations of OC, EC, and TC were observed at both sites.
20 The semi-empirical EC-tracer method was used to derive primary and secondary organic carbons at T1 and T2. The mass loadings of EC, OC, SOC, and POC were comparable to other big cities in the world. EC and OC, including SOC and POC, were influenced by local traffic patterns at T1 and T2, as well as meteorological conditions.
25 Characteristics of OC, EC, SOC, and POC during T1 to T2 transport possible and likely days differed from transport unlikely days. The stronger similarities of SOC and POC between T1 and T2 under transport favorable conditions indicate that particle trans-

Primary and secondary organic carbon downwind of Mexico City

X.-Y. Yu et al.

Title Page

Abstract

Introduction

Conclusions

References

Tables

Figures



Back

Close

Full Screen / Esc

Printer-friendly Version

Interactive Discussion

port occurred. EC, OC, SOC and POC were investigated with respect to trace gas pollutants measured at T1. Strong correlations of EC and POC vs. CO, NO, and NO_x, respectively were observed, indicating primary influence of local traffic emissions. The EC/CO value was determined as 0.0045 at T1. Correlations were also seen between OC and SOC vs. the odd oxygen or the sum of O₃ and NO₂, further confirming the secondary nature of carbons observed at T1.

Acknowledgements. The work was supported by the Office of Science (BER), US Department of Energy, under the auspices of the Atmospheric Science Program, under Contract DE-AC05-76RL01830 at the Pacific Northwest National Laboratory. Meteorological data from T1 were provided by Richard Coulter at Argonne National Laboratory; and meteorological data from T2 by Christopher Doran, William Shaw and Mikhial Pekour at Pacific Northwest National Laboratory. Trace gas data from T1 were provided by the research groups of Gregory Huey of the Georgia Institute of Technology and Ronald Cohen of the University of California, Berkeley. The authors thank Carl Berkowitz and Jerome Fast of Pacific Northwest National Laboratory for useful discussions about emission sources.

References

- Allen, G. A., Lawrence, J., and Koutrakis, P.: Field validation of a semi-continuous method for aerosol black carbon (aethalometer) and temporal patterns of summertime hourly black carbon measurements in southwestern PA, *Atmos. Environ.*, 33(5), 817–823, 1999.
- Bauer, J. J., Yu, X.-Y., Laulainen, N. S., et al.: Characterization of the Sunset Semi-Continuous Carbon Aerosol Analyzer, *J. Air Waste Management Assoc.*, accepted, 2009.
- Birch, M. E.: Analysis of carbonaceous aerosols: interlaboratory comparison, *Analyst*, 123(5), 851–857, 1998.
- Cachier, H., Bremond, M. P., and Buatmenard, P.: Thermal separation of soot carbon, *Aerosol Sci. Tech.*, 10(2), 358–64, 1989.
- Cao, J. J., Lee, S. C., Ho, K. F., et al.: Characteristics of carbonaceous aerosol in Pearl River Delta Region, China during 2001 winter period, *Atmos. Environ.*, 37(11), 1451–1460, 2003.
- Castro, L. M., Pio, C. A., Harrison, R. M., et al.: Carbonaceous aerosol in urban and rural

Primary and secondary organic carbon downwind of Mexico City

X.-Y. Yu et al.

Title Page

Abstract

Introduction

Conclusions

References

Tables

Figures

⏪

⏩

◀

▶

Back

Close

Full Screen / Esc

Printer-friendly Version

Interactive Discussion

**Primary and
secondary organic
carbon downwind of
Mexico City**X.-Y. Yu et al.

[Title Page](#)[Abstract](#)[Introduction](#)[Conclusions](#)[References](#)[Tables](#)[Figures](#)[⏪](#)[⏩](#)[◀](#)[▶](#)[Back](#)[Close](#)[Full Screen / Esc](#)[Printer-friendly Version](#)[Interactive Discussion](#)

European atmospheres: estimation of secondary organic carbon concentrations, *Atmos. Environ.*, 33(17), 2771–2781, 1999.

Chen, G., Huey, L. G., Trainer, M., et al.: An investigation of the chemistry of ship emission plumes during ITCT 2002, *J. Geophys. Res.-Atmos.*, 110(D10), D10S90, doi:10.1029/2004JD005236, 2005.

Chen, L. W. A., Doddridge, B. G., Dickerson, R. R., et al.: Seasonal variations in elemental carbon aerosol, carbon monoxide and sulfur dioxide: Implications for sources, *Geophys. Res. Lett.*, 28(9), 1711–1714, 2001.

Chow, J. C., Watson, J. G., Fujita, E. M., et al.: Temporal and spatial variations of Pm(2.5) and Pm(10) aerosol in the Southern California air-quality study, *Atmos. Environ.*, 28(12), 2061–2080, 1994.

Chow, J. C., Watson, J. G., Crow, D., et al.: Comparison of IMPROVE and NIOSH carbon measurements, *Aerosol Sci. Tech.*, 34(1), 23–34, 2001.

Chow, J. C., Watson, J. G., Edgerton, S. A., et al.: Chemical composition of PM_{2.5} and PM₁₀ in Mexico City during winter 1997, *Sci. Total Environ.*, 287(3), 177–201, 2002.

Chow, J. C., Watson, J. G., Lowenthal, D. H., et al.: Particulate carbon measurements in California's San Joaquin Valley, *Chemosphere*, 62(3), 337–348, 2006.

Chu, S. H.: Stable estimate of primary OC/EC ratios in the EC tracer method, *Atmos. Environ.*, 39(8), 1383–1392, 2005.

Cornbleet, P. J. and Gochman, N.: Incorrect Least-Squares Regression Coefficients in Method-Comparison Analysis, *Clin. Chem.*, 25(3), 432–438, 1979.

Dan, M., Zhuang, G. S., Li, X. X., et al.: The characteristics of carbonaceous species and their sources in PM_{2.5} in Beijing, *Atmos. Environ.*, 38(21), 3443–3452, 2004.

Doran, J. C., Barnard, J. C., Arnott, W. P., Cary, R., Coulter, R., Fast, J. D., Kassianov, E. I., Kleinman, L., Laulainen, N. S., Martin, T., Paredes-Miranda, G., Pekour, M. S., Shaw, W. J., Smith, D. F., Springston, S. R., and Yu, X.-Y.: The T1-T2 study: evolution of aerosol properties downwind of Mexico City, *Atmos. Chem. Phys.*, 7, 1585–1598, 2007, <http://www.atmos-chem-phys.net/7/1585/2007/>.

Duan, F. K., He, K. B., Ma, Y. L., et al.: Characteristics of carbonaceous aerosols in Beijing, China, *Chemosphere*, 60(3), 355–364, 2005.

Fast, J. D., de Foy, B., Acevedo Rosas, F., Caetano, E., Carmichael, G., Emmons, L., McKenna, D., Mena, M., Skamarock, W., Tie, X., Coulter, R. L., Barnard, J. C., Wiedinmyer, C., and Madronich, S.: A meteorological overview of the MILAGRO field campaigns, *Atmos. Chem.*

- Phys., 7, 2233–2257, 2007,
<http://www.atmos-chem-phys.net/7/2233/2007/>.
- Feng, J. L., Hu, M., Chan, C. K., et al.: A comparative study of the organic matter in PM_{2.5} from three Chinese megacities in three different climatic zones, *Atmos. Environ.*, 40(21), 3983–3994, 2006.
- 5 Gelencser, A., May, B., Simpson, D., et al.: Source apportionment of PM_{2.5} organic aerosol over Europe: Primary/secondary, natural/anthropogenic, and fossil/biogenic origin, *J. Geophys. Res.-Atmos.*, 112(D23), D23S04, doi:10.1029/2006JD008094, 2007.
- Harley, R. A., Marr, L. C., Lehner, J. K., et al.: Changes in motor vehicle emissions on diurnal to decadal time scales and effects on atmospheric composition, *Environ. Sci. Tech.*, 39(14), 5356–5362, 2005.
- 10 Hennigan, C. J., Sullivan, A. P., Fountoukis, C. I., Nenes, A., Hecobian, A., Vargas, O., Peltier, R. E., Case Hanks, A. T., Huey, L. G., Lefer, B. L., Russell, A. G., and Weber, R. J.: On the volatility and production mechanisms of newly formed nitrate and water soluble organic aerosol in Mexico City, *Atmos. Chem. Phys.*, 8, 3761–3768, 2008,
<http://www.atmos-chem-phys.net/8/3761/2008/>.
- 15 Herndon, S. C., Onasch, T. B., Wood, E. C., et al.: Correlation of secondary organic aerosol with odd oxygen in Mexico City, *Geophys. Res. Lett.*, 35, L15804, doi:10.1029/2008GL034058, 2008.
- 20 Hildemann, L. M., Rogge, W. F., Cass, G. R., et al.: Contribution of primary aerosol emissions from vegetation-derived sources to fine particle concentrations in Los Angeles, *J. Geophys. Res.-Atmos.*, 101(D14), 19541–19549, 1996.
- Ho, K. F., Lee, S. C., Yu, J. C., et al.: Carbonaceous characteristics of atmospheric particulate matter in Hong Kong, *Sci. Total Environ.*, 300(1–3), 59–67, 2002.
- 25 Jeong, C. H., Hopke, P. K., Kim, E., et al.: The comparison between thermal-optical transmittance elemental carbon and Aethalometer black carbon measured at multiple monitoring sites, *Atmos. Environ.*, 38(31), 5193–5204, 2004.
- Kondo, Y., Miyazaki, Y., Takegawa, N., et al.: Oxygenated and water-soluble organic aerosols in Tokyo, *J. Geophys. Res.-Atmos.*, 112(D1), D01203, doi:10.1029/2006JD007056, 2007.
- 30 Lim, H. J. and Turpin, B. J.: Origins of primary and secondary organic aerosol in Atlanta: Results of time-resolved measurements during the Atlanta supersite experiment, *Environ. Sci. Tech.*, 36(21), 4489–4496, 2002.
- Lonati, G., Ozgen, S., and Giugliano, M.: Primary and secondary carbonaceous species in

**Primary and
secondary organic
carbon downwind of
Mexico City**X.-Y. Yu et al.

Title Page

Abstract

Introduction

Conclusions

References

Tables

Figures

◀

▶

◀

▶

Back

Close

Full Screen / Esc

Printer-friendly Version

Interactive Discussion

- PM_{2.5} samples in Milan (Italy), *Atmos. Environ.*, 41(22), 4599–4610, 2007.
- Martin, R.: General deming regression for estimating systematic bias and its confidence interval in method-comparison studies, *Clin. Chem.*, 46(1), 100–104, 2000.
- Nunnermacker, L. J., Imre, D., Daum, P. H., et al.: Characterization of the Nashville urban plume on July 3 and July 18, 1995, *J. Geophys. Res.-Atmos.*, 103(D21), 28129–28148, 1998.
- Pandis, S. N., Harley, R. A., Cass, G. R., et al.: Secondary organic aerosol formation and transport, *Atmos. Environ. A-Gen.*, 26(13), 2269–2282, 1992.
- Park, S. S., Bae, M. S., Schauer, J. J., et al.: Evaluation of the TMO and TOT methods for OC and EC measurements and their characteristics in PM_{2.5} at an urban site of Korea during ACE-Asia, *Atmos. Environ.*, 39(28), 5101–5112, 2005a.
- Park, S. S., Harrison, D., Pancras, J. P., et al.: Highly time-resolved organic and elemental carbon measurements at the Baltimore Supersite in 2002, *J. Geophys. Res.-Atmos.*, 110(D7), D07S06, doi:10.1029/2004JD004610, 2005b.
- Plaza, J., Gomez-Moreno, F. J., Nunez, L., et al.: Estimation of secondary organic aerosol formation from semicontinuous OC-EC measurements in a Madrid suburban area, *Atmos. Environ.*, 40(6), 1134–1147, 2006.
- Querol, X., Pey, J., Minguillón, M. C., Pérez, N., Alastuey, A., Viana, M., Moreno, T., Bernabé, R. M., Blanco, S., Cárdenas, B., Vega, E., Sosa, G., Escalona, S., Ruiz, H., and Artíñano, B.: PM speciation and sources in Mexico during the MILAGRO-2006 Campaign, *Atmos. Chem. Phys.*, 8, 111–128, 2008, <http://www.atmos-chem-phys.net/8/111/2008/>.
- Russell, M. and Allen, D. T.: Seasonal and spatial trends in primary and secondary organic carbon concentrations in southeast Texas, *Atmos. Environ.*, 38(20), 3225–3239, 2004.
- Salma, I., Chi, X. G., and Maenhaut, W.: Elemental and organic carbon in urban canyon and background environments in Budapest, Hungary, *Atmos. Environ.*, 38(1), 27–36, 2004.
- Saylor, R. D., Edgerton, E. S., and Hartsell, B. E.: Linear regression techniques for use in the EC tracer method of secondary organic aerosol estimation, *Atmos. Environ.*, 40(39), 7546–7556, 2006.
- Schauer, J. J., Rogge, W. F., Hildemann, L. M., et al.: Source apportionment of airborne particulate matter using organic compounds as tracers, *Atmos. Environ.*, 30(22), 3837–3855, 1996.
- Schauer, J. J., Kleeman, M. J., Cass, G. R., et al.: Measurement of emissions from air pollution sources. 5. C1–C32 organic compounds from gasoline-powered motor vehicles, *Environ.*

Primary and secondary organic carbon downwind of Mexico CityX.-Y. Yu et al.

[Title Page](#)[Abstract](#)[Introduction](#)[Conclusions](#)[References](#)[Tables](#)[Figures](#)[⏪](#)[⏩](#)[◀](#)[▶](#)[Back](#)[Close](#)[Full Screen / Esc](#)[Printer-friendly Version](#)[Interactive Discussion](#)

**Primary and
secondary organic
carbon downwind of
Mexico City**X.-Y. Yu et al.

Sci. Tech., 36(6), 1169–1180, 2002.

Schauer, J. J., Mader, B. T., Deminter, J. T., et al.: ACE-Asia intercomparison of a thermal-optical method for the determination of particle-phase organic and elemental carbon, *Environ. Sci. Tech.*, 37(5), 993–1001, 2003.

5 Schichtel, B. A., Malm, W. C., Bench, G., et al.: Fossil and contemporary fine particulate carbon fractions at 12 rural and urban sites in the United States, *J. Geophys. Res.-Atmos.*, 113(D2), D02311, doi:10.1029/2007JD008605, 2008.

Shaw, W. J., Pekour, M. S., Coulter, R. L., Martin, T. J., and Walters, J. T.: The daytime mixing layer observed by radiosonde, profiler, and lidar during MILAGRO, *Atmos. Chem. Phys. Discuss.*, 7, 15025–15065, 2007,
10 <http://www.atmos-chem-phys-discuss.net/7/15025/2007/>.

Stone, E. A., Snyder, D. C., Sheesley, R. J., Sullivan, A. P., Weber, R. J., and Schauer, J. J.: Source apportionment of fine organic aerosol in Mexico City during the MILAGRO experiment 2006, *Atmos. Chem. Phys.*, 8, 1249–1259, 2008,
15 <http://www.atmos-chem-phys.net/8/1249/2008/>.

Strader, R., Lurmann, F., and Pandis, S. N.: Evaluation of secondary organic aerosol formation in winter, *Atmos. Environ.*, 33(29), 4849–4863, 1999.

Sullivan, A. P., Peltier, R. E., Brock, C. A., et al.: Airborne measurements of carbonaceous aerosol soluble in water over northeastern United States: Method development and an investigation into water-soluble organic carbon sources, *J. Geophys. Res.-Atmos.*, 111(D23), D23S46, doi:10.1029/2006JD007072, 2006.
20

Takegawa, N., Miyakawa, T., Kondo, Y., et al.: Seasonal and diurnal variations of submicron organic aerosol in Tokyo observed using the Aerodyne aerosol mass spectrometer, *J. Geophys. Res.*, 111, D11206, doi:10.1029/2005JD006515, 2006.

25 Turpin, B. J. and Huntzicker, J. J.: Secondary formation of organic aerosol in the Los-Angeles basin – A descriptive analysis of organic and elemental carbon concentrations, *Atmos. Environ. A-Gen.*, 25(2), 207–215, 1991.

Turpin, B. J., Huntzicker, J. J., Larson, S. M., et al.: Los-Angeles summer midday particulate carbon – primary and secondary aerosol, *Environ. Sci. Tech.*, 25(10), 1788–1793, 1991.

30 Turpin, B. J. and Huntzicker, J. J.: Identification of Secondary Organic Aerosol Episodes and Quantitation of Primary and Secondary Organic Aerosol Concentrations During Scaqs, *Atmos. Environ.*, 29(23), 3527–3544, 1995.

Viana, M., Maenhaut, W., ten Brink, H. M., et al.: Comparative analysis of organic and ele-

[Title Page](#)[Abstract](#)[Introduction](#)[Conclusions](#)[References](#)[Tables](#)[Figures](#)[⏪](#)[⏩](#)[◀](#)[▶](#)[Back](#)[Close](#)[Full Screen / Esc](#)[Printer-friendly Version](#)[Interactive Discussion](#)

- mental carbon concentrations in carbonaceous aerosols in three European cities, *Atmos. Environ.*, 41(28), 5972–5983, 2007.
- Wang, T., Wong, C. H., Cheung, T. F., et al.: Relationships of trace gases and aerosols and the emission characteristics at Lin'an, a rural site in eastern China, during spring 2001, *J. Geophys. Res.-Atmos.*, 109(D19), 2004.
- 5 Watson, J. G. and Chow, J. C.: A wintertime PM_{2.5} episode at the Fresno, CA, supersite, *Atmos. Environ.*, 36(3), 465–475, 2002.
- Yu, J. H., Chen, T., Guinot, B., et al.: Characteristics of carbonaceous particles in Beijing during winter and summer 2003, *Adv. Atmos. Sci.*, 23(3), 468–473, 2006.
- 10 Yu, J. Z., Tung, J. W. T., Wu, A. W. M., et al.: Abundance and seasonal characteristics of elemental and organic carbon in Hong Kong PM₁₀, *Atmos. Environ.*, 38(10), 1511–1521, 2004a.
- Yu, S., Bhave, P. V., Dennis, R. L., et al.: Seasonal and regional variations of primary and secondary organic aerosols over the Continental United States: Semi-empirical estimates and model evaluation, *Environ. Sci. Tech.*, 41(13), 4690–4697, 2007.
- 15 Yu, S. C., Dennis, R. L., Bhave, P. V., et al.: Primary and secondary organic aerosols over the United States: estimates on the basis of observed organic carbon (OC) and elemental carbon (EC), and air quality modeled primary OC/EC ratios, *Atmos. Environ.*, 38(31), 5257–5268, 2004b.
- 20 Yuan, Z. B., Yu, J. Z., Lau, A. K. H., Louie, P. K. K., and Fung, J. C. H.: Application of positive matrix factorization in estimating aerosol secondary organic carbon in Hong Kong and its relationship with secondary sulfate, *Atmos. Chem. Phys.*, 6, 25–34, 2006, <http://www.atmos-chem-phys.net/6/25/2006/>.

**Primary and
secondary organic
carbon downwind of
Mexico City**

X.-Y. Yu et al.

Title Page

Abstract

Introduction

Conclusions

References

Tables

Figures

⏪

⏩

◀

▶

Back

Close

Full Screen / Esc

Printer-friendly Version

Interactive Discussion

**Primary and
secondary organic
carbon downwind of
Mexico City**

X.-Y. Yu et al.

Table 1. The modified NIOSH 5040 thermal-optical protocol used during the MILAGRO campaign.

Carrier gas	Duration (s)	Temperature (°C)
He-1	10	Ambient
He-2	80	600
He-3	90	870
He-4	25	No Heat
O ₂ -1	30	600
O ₂ -2	30	700
O ₂ -3	35	760
O ₂ -4	105	870
CalGas	110	No Heat

[Title Page](#)[Abstract](#)[Introduction](#)[Conclusions](#)[References](#)[Tables](#)[Figures](#)[◀](#)[▶](#)[◀](#)[▶](#)[Back](#)[Close](#)[Full Screen / Esc](#)[Printer-friendly Version](#)[Interactive Discussion](#)

**Primary and
secondary organic
carbon downwind of
Mexico City**

X.-Y. Yu et al.

Table 2. Summary of linear least-squares fit parameters between quantities determined using optical and thermal-optical approaches.

Species	Optical vs. Thermal	T1	T2
OC	Slope	0.93±0.01	0.84±0.02
	R^2	0.95	0.37
EC	Slope	1.43±0.01	1.39±0.01
	R^2	0.96	0.91

Title Page

Abstract

Introduction

Conclusions

References

Tables

Figures

◀

▶

◀

▶

Back

Close

Full Screen / Esc

Printer-friendly Version

Interactive Discussion

**Primary and
secondary organic
carbon downwind of
Mexico City**

X.-Y. Yu et al.

Table 3. Statistical summary at T1 and T2.

T1	Thermal OC $\mu\text{g C}/\text{m}^3$	Thermal EC $\mu\text{g C}/\text{m}^3$	Thermal TC $\mu\text{g C}/\text{m}^3$	EC:TC
average	6.3	2.0	8.4	0.17
standard deviation	3.0	1.8	4.4	0.08
maximum	29.3	13.3	40.5	0.5
minimum	1.1	0	1.2	0
T2				
average	4.9	0.4	5.4	0.06
standard deviation	2.2	0.4	2.4	0.04
maximum	15.1	1.9	16.7	0.2
minimum	0.8	0	1.0	0

Title Page

Abstract

Introduction

Conclusions

References

Tables

Figures

⏪

⏩

◀

▶

Back

Close

Full Screen / Esc

Printer-friendly Version

Interactive Discussion

**Primary and
secondary organic
carbon downwind of
Mexico City**

X.-Y. Yu et al.

Table 4. Summary of global linear least-squares fits of Thermal OC vs. Thermal EC at T1 and T2.

Site	Fitting Functions	Thermal OC vs. Thermal EC	
		Linear Least-squares	Deming Least-squares
T1	Slope	0.74±0.07	0.93±0.14
	Intercept	4.77±0.19	4.39±0.26
	R^2	0.20	–
T2	Slope	3.79±0.12	4.30±0.36
	Intercept	3.25±0.12	3.02±0.15
	R^2	0.45	–

– R^2 is not available as an output of the Deming regression analysis program.

Title Page

Abstract

Introduction

Conclusions

References

Tables

Figures

⏪

⏩

◀

▶

Back

Close

Full Screen / Esc

Printer-friendly Version

Interactive Discussion

Primary and secondary organic carbon downwind of Mexico City

X.-Y. Yu et al.

Table 5. Comparison of PM_{2.5} OC:EC, OC, EC, and TC observed in different cities.

Location	Duration	OC:EC	OC avg	EC avg μg C/m ³	TC	Season	Method	Reference
Beijing	~2 weeks	2.4	9.4	4.3	–	Summer	Rupprecht ambient carbon particulate monitor	Yu et al. (2006)
Beijing	~3 months	3.0	20.4	6.6	26.9	Fall	Rupprecht ambient carbon particulate monitor	Duan et al. (2005)
Shanghai	1 week	–	7.9	3.5	11.4	Summer	Sunset OCEC analyzer NIOSH protocol	Feng et al. (2006)
Guangzhou	1 week	–	14.5	6.3	20.8	Summer	Sunset OCEC analyzer NIOSH protocol	Feng et al. (2006)
Hong Kong	~4 months	2–3	12	6	–	Winter	Thermal manganese dioxide oxidation	Ho et al. (2002)
Hong Kong	~2 months	2.4	14.7	6.1	–	Winter	IMPROVE thermal optical reflectance method	Cao et al. (2003)
Houston	~2 years	2.9–4.8	2.4–4.3	0.3–0.6	–	All	NIOSH thermal optical reflectance method	Russell and Allen (2004)
Los Angeles	~4 months	2.5	8.3	2.4	2–	Summer	IMPROVE thermal optical reflectance method	Chow et al. (1994)
Milan	~5 month	4.2	5.2	1.2	–	Summer	NIOSH thermal optical reflectance method	Lonati et al. (2007)
Madrid	~1 month	2.7	4	1	–	Summer	EPA thermo optical transmittance technique	Plaza et al. (2006)
Barcelona	~5 weeks	2.8	3.9	1.9	5.8	Summer	Sunset OCEC analyzer NIOSH protocol	Viana et al. (2007)
Amsterdam	~5 weeks	2.6	3.6	1.5	5.1	Summer	Sunset OCEC analyzer NIOSH protocol	Viana et al. (2007)
US rural	~2 years	2.3–4.0*	–	–	–	Summer	IMPROVE thermal optical reflectance method	Schichtel et al. (2008)
US urban	~2 years	1.1–1.7*	–	–	–	Summer	IMPROVE thermal optical reflectance method	Schichtel et al. (2008)
Mexico	~3 weeks	1.7**	9.9	5.8	15.8	Spring	IMPROVE thermal optical reflectance method	Chow et al. (2002)
Mexico-T1	~4 weeks	–	3.7	4.0	16	Spring	IMPROVE thermal optical reflectance method	Querol et al. (2008)
Mexico-T1	~4 weeks	0.9	6.3	2.0	8.4	Spring	Sunset OCEC analyzer modified NIOSH protocol	This work
Mexico-T2	~4 weeks	4.3	4.9	0.4	5.4	Spring	Sunset OCEC analyzer modified NIOSH protocol	This work

* Derived from EC/TC 82nd–98th percentile ratios

** Derived from OC/TC

– Not available from original references

Title Page

Abstract

Introduction

Conclusions

References

Tables

Figures

⏪

⏩

◀

▶

Back

Close

Full Screen / Esc

Printer-friendly Version

Interactive Discussion

**Primary and
secondary organic
carbon downwind of
Mexico City**

X.-Y. Yu et al.

Table 6. Summary of linear least-squares fitting results grouped by the lowest percentage of OC:EC ratios at T1 and T2.

Site	Lowest % by OC:EC	No. of data	Slope	Intercept	R^2
T1	2.5%	12	0.49±0.09	2.66±0.77	0.75
	5%	25	0.64±0.10	2.07±0.71	0.65
	10%	50	0.64±0.08	2.69±0.46	0.58
T2	2.5%	12	2.82±0.53	0.54±0.61	0.74
	5%	24	3.43±0.46	0.64±0.48	0.71
	10%	48	3.71±0.41	1.14±0.37	0.62

Title Page

Abstract

Introduction

Conclusions

References

Tables

Figures

⏪

⏩

◀

▶

Back

Close

Full Screen / Esc

Printer-friendly Version

Interactive Discussion

Primary and secondary organic carbon downwind of Mexico City

X.-Y. Yu et al.

[Title Page](#)[Abstract](#)[Introduction](#)[Conclusions](#)[References](#)[Tables](#)[Figures](#)[I◀](#)[▶I](#)[◀](#)[▶](#)[Back](#)[Close](#)[Full Screen / Esc](#)[Printer-friendly Version](#)[Interactive Discussion](#)

Table 7. Summary of linear least-squares fitting results to determine the minimum OC:EC ratios at T1 and T2.

Site	No. of data	Slope	Intercept	R^2
T1	36	0.61 ± 0.02	1.63 ± 0.12	0.95
T2	12	2.26 ± 0.28	0.76 ± 0.28	0.86

**Primary and
secondary organic
carbon downwind of
Mexico City**

X.-Y. Yu et al.

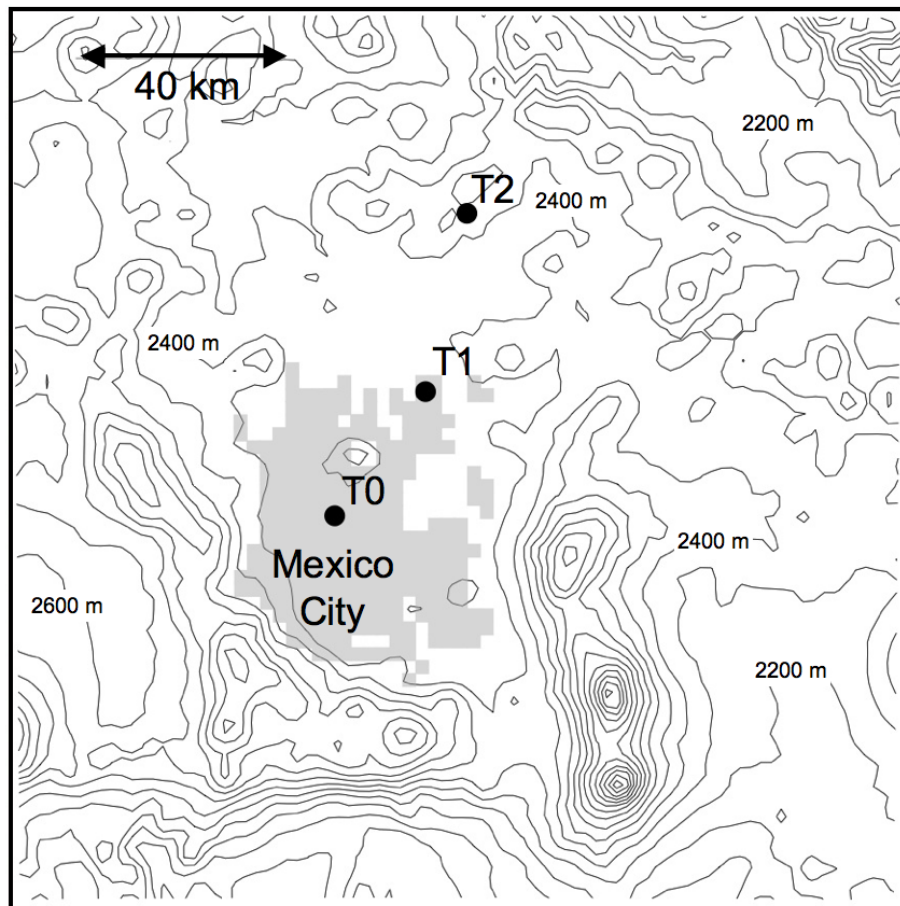


Fig. 1. Site map showing T0, T1, and T2 in relation to Mexico City.

[Title Page](#)[Abstract](#)[Introduction](#)[Conclusions](#)[References](#)[Tables](#)[Figures](#)[⏪](#)[⏩](#)[◀](#)[▶](#)[Back](#)[Close](#)[Full Screen / Esc](#)[Printer-friendly Version](#)[Interactive Discussion](#)

**Primary and
secondary organic
carbon downwind of
Mexico City**

X.-Y. Yu et al.

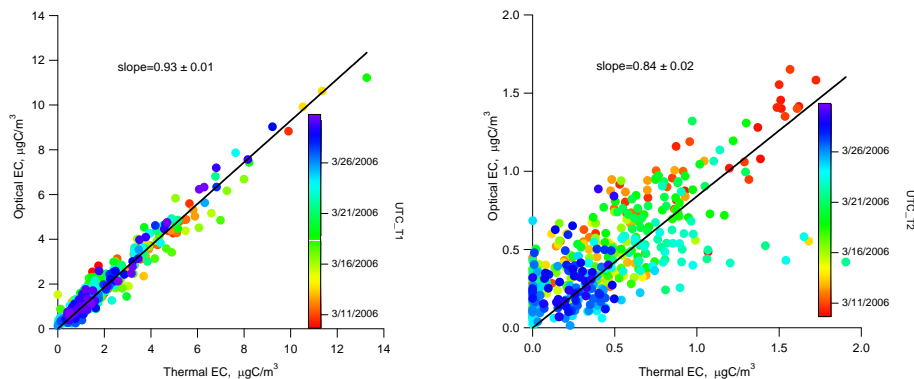


Fig. 2a. Scatter plots of Optical EC vs. Thermal EC at T1 (left panel) and T2 (right panel). The solid lines are linear least-squares fits.

[Title Page](#)[Abstract](#)[Introduction](#)[Conclusions](#)[References](#)[Tables](#)[Figures](#)[⏪](#)[⏩](#)[◀](#)[▶](#)[Back](#)[Close](#)[Full Screen / Esc](#)[Printer-friendly Version](#)[Interactive Discussion](#)

**Primary and
secondary organic
carbon downwind of
Mexico City**

X.-Y. Yu et al.

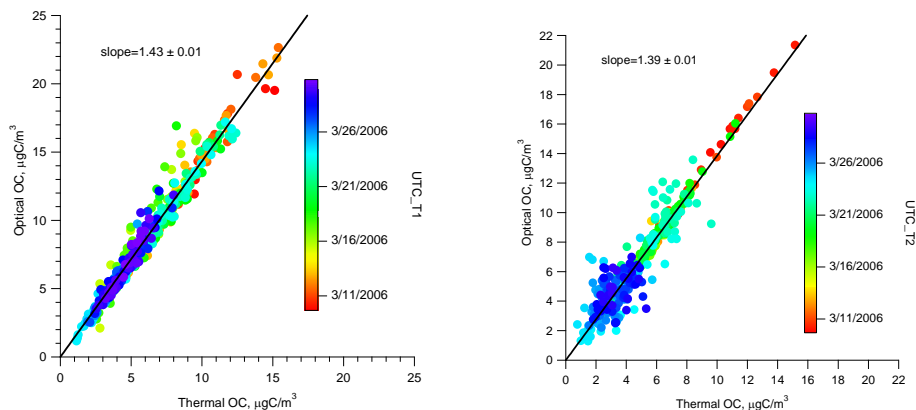


Fig. 2b. Scatter plots of Optical OC vs. Thermal OC at T1 (left panel) and T2 (right panel). The solids lines are linear least-squares fits.

[Title Page](#)[Abstract](#)[Introduction](#)[Conclusions](#)[References](#)[Tables](#)[Figures](#)[⏪](#)[⏩](#)[◀](#)[▶](#)[Back](#)[Close](#)[Full Screen / Esc](#)[Printer-friendly Version](#)[Interactive Discussion](#)

Primary and secondary organic carbon downwind of Mexico City

X.-Y. Yu et al.

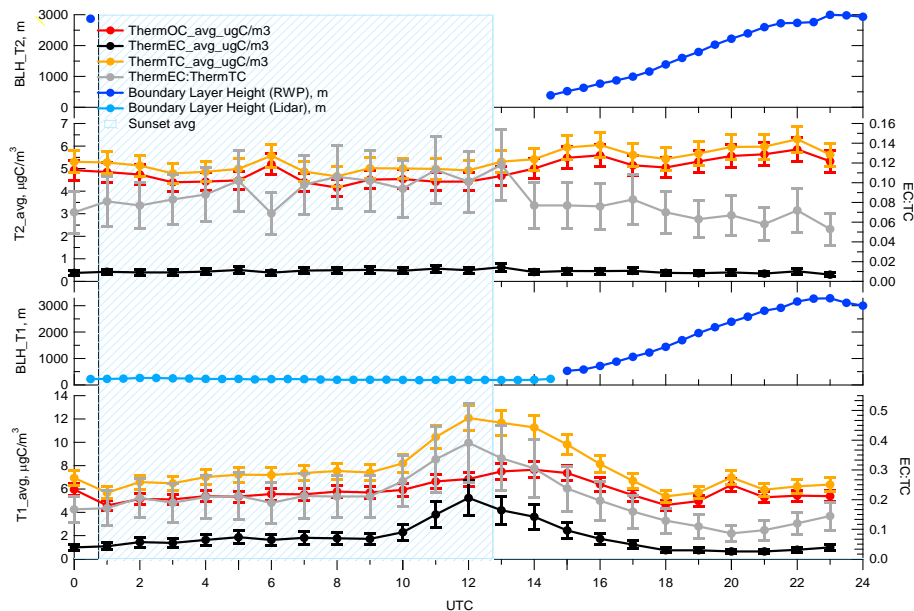


Fig. 3. Monthly average of Thermal EC, Thermal OC, and Thermal TC, shown on the left axis; and the ratios of Thermal EC: Thermal TC shown on the right axis. The top panel depicts data from T2, and the bottom panel depicts data from T1.

Title Page

Abstract

Introduction

Conclusions

References

Tables

Figures

◀

▶

◀

▶

Back

Close

Full Screen / Esc

Printer-friendly Version

Interactive Discussion

Primary and secondary organic carbon downwind of Mexico City

X.-Y. Yu et al.

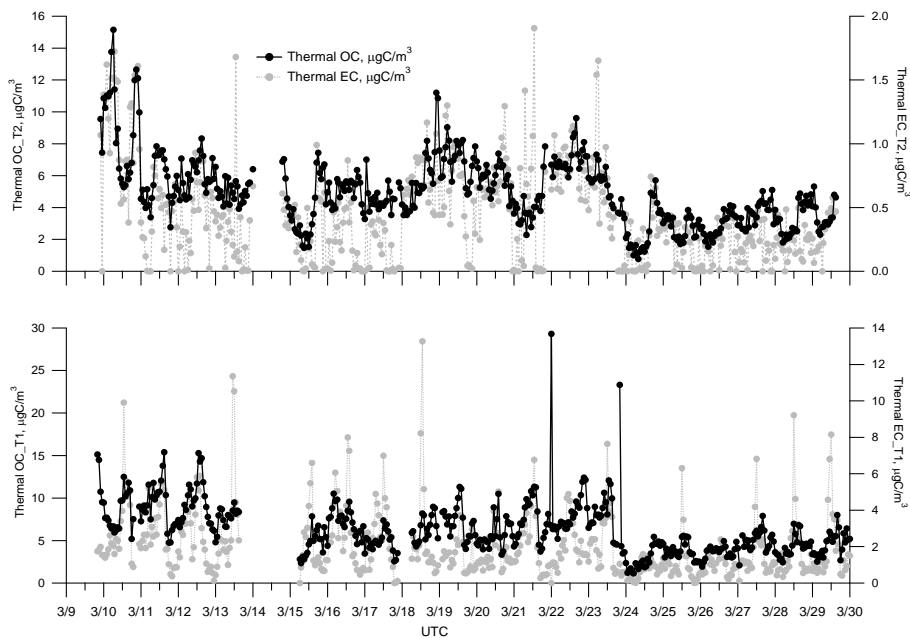


Fig. 4. Time series of Thermal OC (black dots) and Thermal EC (light grey dots) at T1 and T2 sites.

Title Page

Abstract

Introduction

Conclusions

References

Tables

Figures

◀

▶

◀

▶

Back

Close

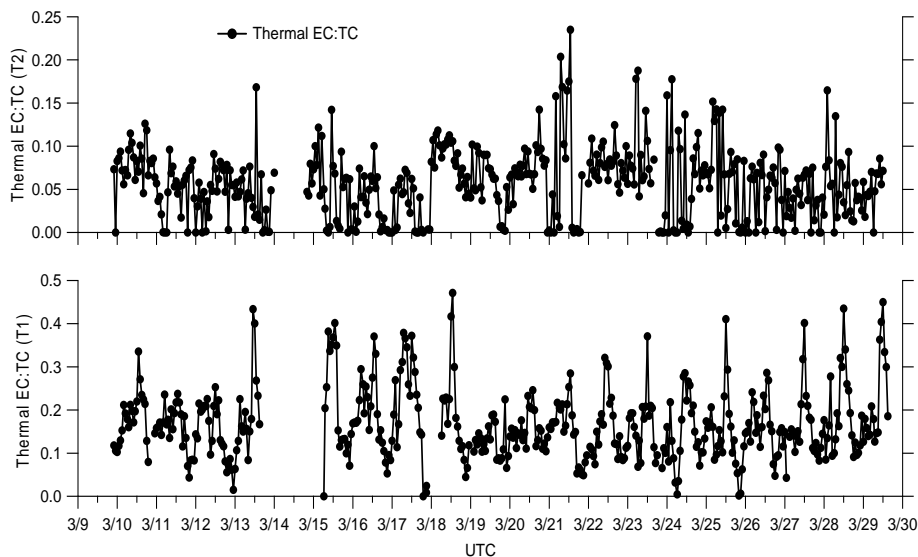
Full Screen / Esc

Printer-friendly Version

Interactive Discussion

**Primary and
secondary organic
carbon downwind of
Mexico City**

X.-Y. Yu et al.

**Fig. 5a.** Time series of the ratios of Thermal EC to TC.[Title Page](#)[Abstract](#)[Introduction](#)[Conclusions](#)[References](#)[Tables](#)[Figures](#)[⏪](#)[⏩](#)[◀](#)[▶](#)[Back](#)[Close](#)[Full Screen / Esc](#)[Printer-friendly Version](#)[Interactive Discussion](#)

Primary and secondary organic carbon downwind of Mexico City

X.-Y. Yu et al.

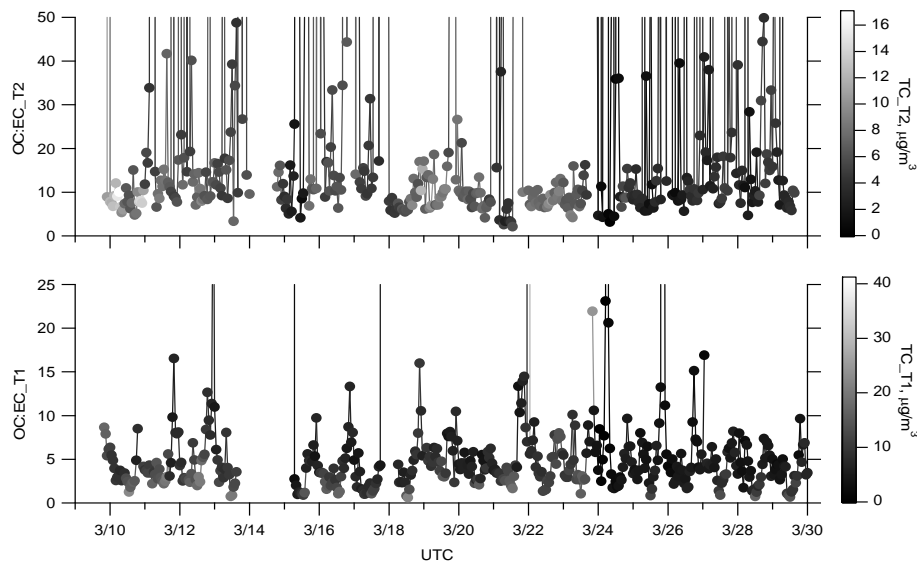


Fig. 5b. Time series of the ratios of Thermal OC to Thermal EC at T1 and T2. The data are shaded as a function of TC mass loading at each site.

[Title Page](#)[Abstract](#)[Introduction](#)[Conclusions](#)[References](#)[Tables](#)[Figures](#)[⏪](#)[⏩](#)[◀](#)[▶](#)[Back](#)[Close](#)[Full Screen / Esc](#)[Printer-friendly Version](#)[Interactive Discussion](#)

Primary and
secondary organic
carbon downwind of
Mexico City

X.-Y. Yu et al.

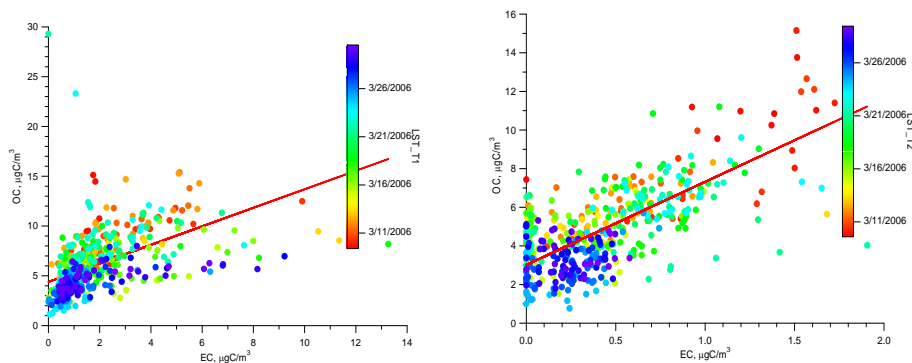


Fig. 6a. Scatter plots of OC vs. EC at T1 (left panel) and T2 (right panel), respectively. The solid lines are the global linear least-squares fits using Deming regression analysis. The data points are color coded as a function of date.

[Title Page](#)[Abstract](#)[Introduction](#)[Conclusions](#)[References](#)[Tables](#)[Figures](#)[⏪](#)[⏩](#)[◀](#)[▶](#)[Back](#)[Close](#)[Full Screen / Esc](#)[Printer-friendly Version](#)[Interactive Discussion](#)

**Primary and
secondary organic
carbon downwind of
Mexico City**

X.-Y. Yu et al.

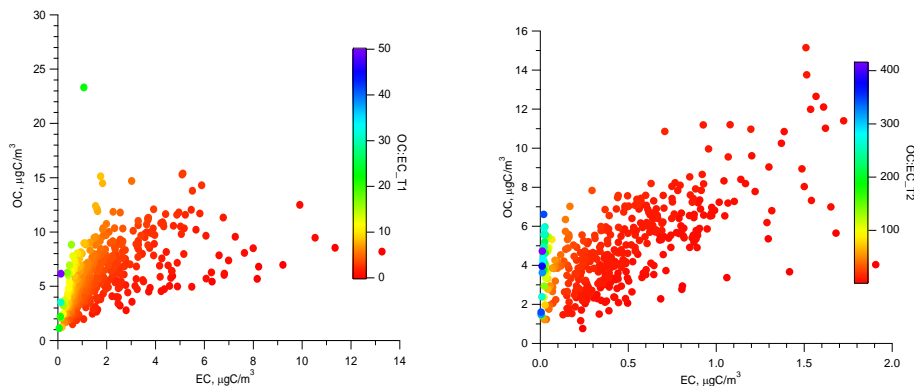


Fig. 6b. Scatter plots of OC vs. EC at T1 (left panel) and T2 (right panel), respectively. The data points are color coded as a function of the OC to EC ratio.

[Title Page](#)[Abstract](#)[Introduction](#)[Conclusions](#)[References](#)[Tables](#)[Figures](#)[⏪](#)[⏩](#)[◀](#)[▶](#)[Back](#)[Close](#)[Full Screen / Esc](#)[Printer-friendly Version](#)[Interactive Discussion](#)

Primary and secondary organic carbon downwind of Mexico City

X.-Y. Yu et al.

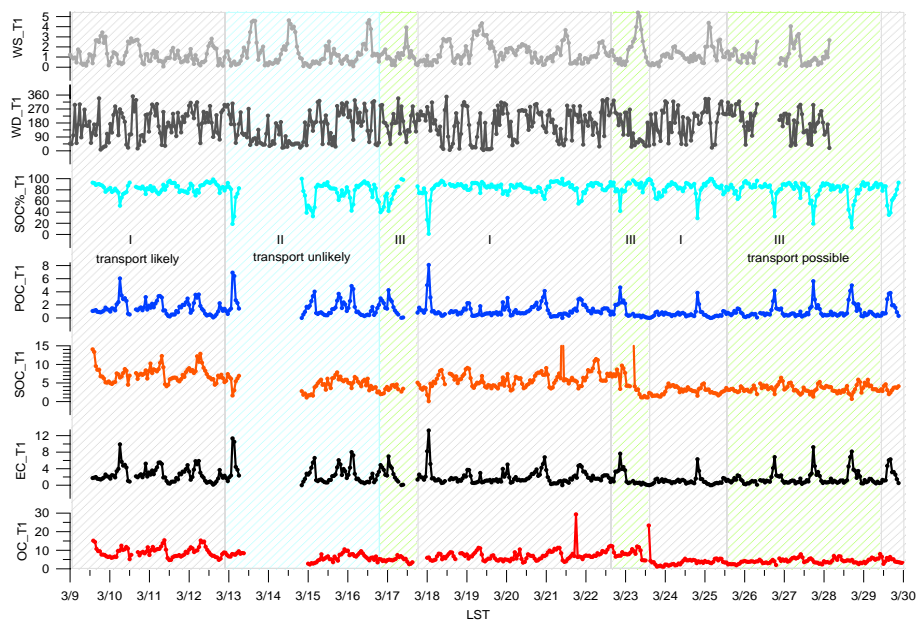


Fig. 7a. Time series of OC, EC, POC, SOC, SOC%, wind direction, and wind speed at T1.

[Title Page](#)[Abstract](#)[Introduction](#)[Conclusions](#)[References](#)[Tables](#)[Figures](#)[◀](#)[▶](#)[◀](#)[▶](#)[Back](#)[Close](#)[Full Screen / Esc](#)[Printer-friendly Version](#)[Interactive Discussion](#)

Primary and secondary organic carbon downwind of Mexico City

X.-Y. Yu et al.

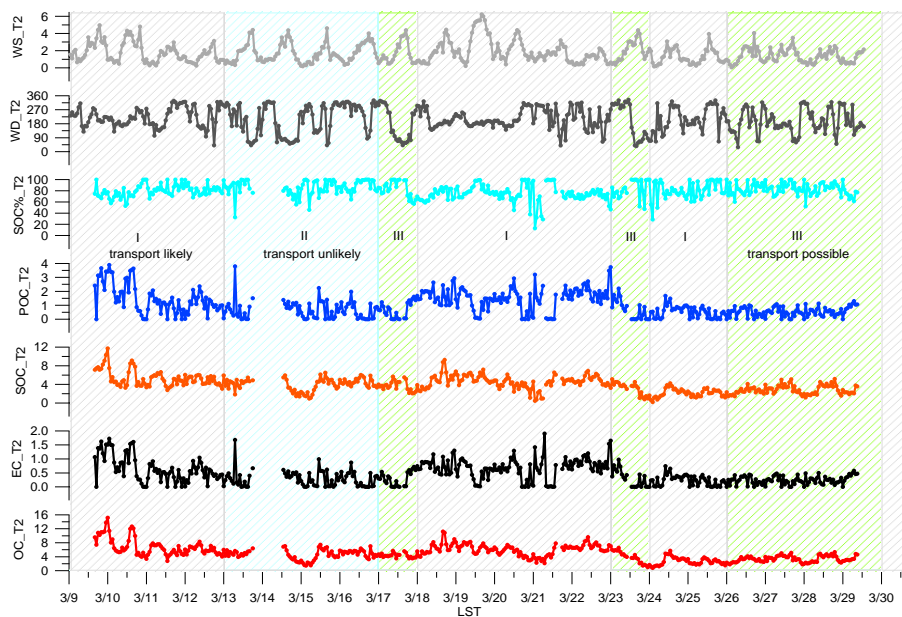


Fig. 7b. Time series of OC, EC, POC, SOC, SOC%, wind direction, and wind speed at T2.

[Title Page](#)[Abstract](#)[Introduction](#)[Conclusions](#)[References](#)[Tables](#)[Figures](#)[◀](#)[▶](#)[◀](#)[▶](#)[Back](#)[Close](#)[Full Screen / Esc](#)[Printer-friendly Version](#)[Interactive Discussion](#)

**Primary and
secondary organic
carbon downwind of
Mexico City**

X.-Y. Yu et al.

Title Page

Abstract

Introduction

Conclusions

References

Tables

Figures

◀

▶

◀

▶

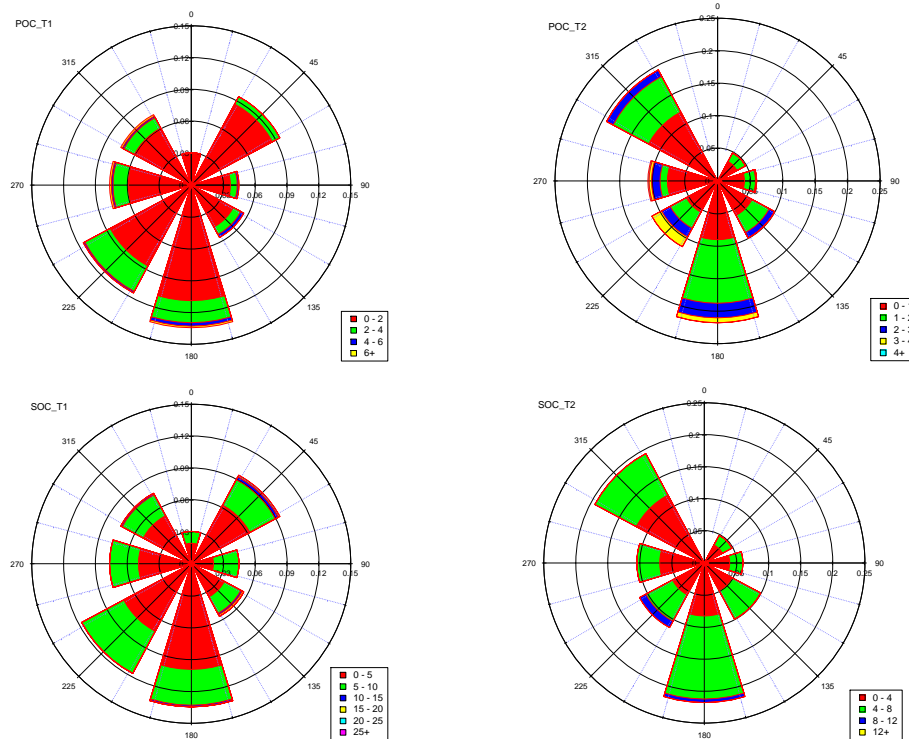
Back

Close

Full Screen / Esc

Printer-friendly Version

Interactive Discussion

**Fig. 8.** Wind roses of POC and SOC at T1 (left) and T2 (right).

**Primary and
secondary organic
carbon downwind of
Mexico City**

X.-Y. Yu et al.

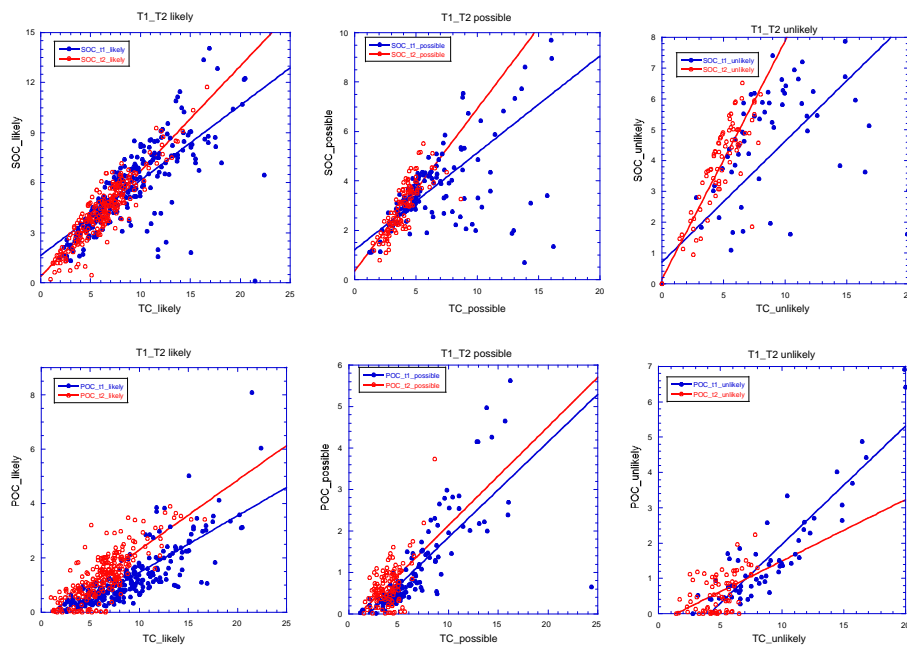


Fig. 9. Scatter plots of SOC vs. TC and POC vs. TC during the three transport scenarios between T1 to T2, transport likely, possible, and unlikely dates. The solid lines are linear least-squares fits.

Title Page

Abstract

Introduction

Conclusions

References

Tables

Figures

◀

▶

◀

▶

Back

Close

Full Screen / Esc

Printer-friendly Version

Interactive Discussion

Primary and secondary organic carbon downwind of Mexico City

X.-Y. Yu et al.

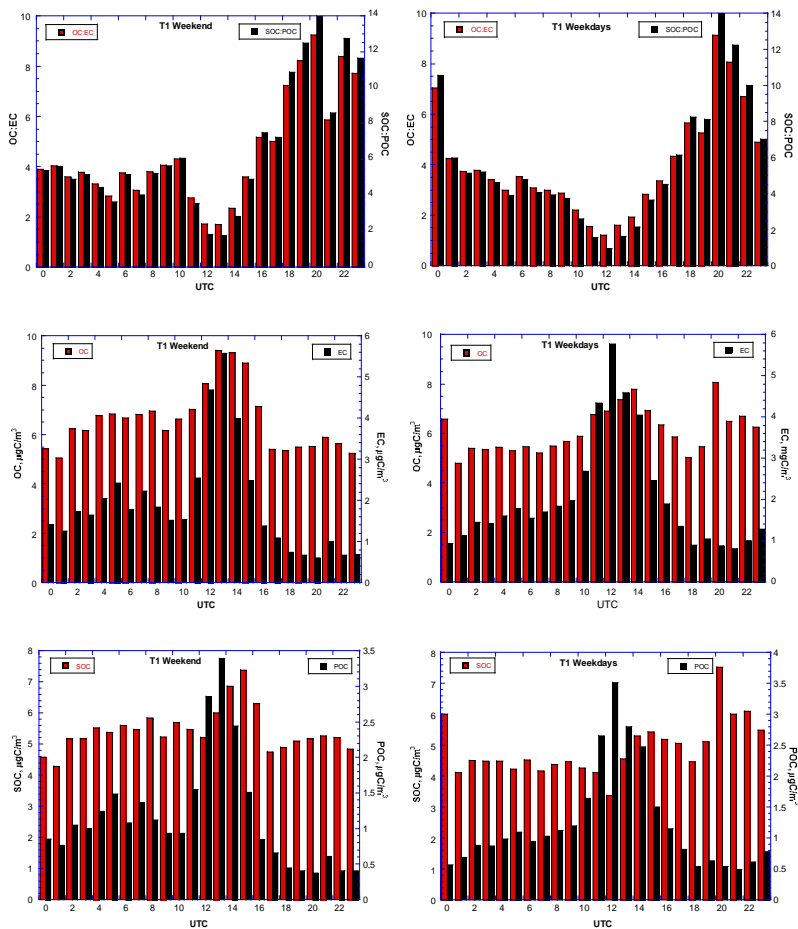


Fig. 10a. Average weekend (left column) and weekday (right column) patterns of OC/EC, SOC/POC, EC, OC, POC, and SOC at T1.

[Title Page](#)
[Abstract](#)
[Introduction](#)
[Conclusions](#)
[References](#)
[Tables](#)
[Figures](#)
[⏪](#)
[⏩](#)
[⏴](#)
[⏵](#)
[Back](#)
[Close](#)
[Full Screen / Esc](#)
[Printer-friendly Version](#)
[Interactive Discussion](#)

Primary and secondary organic carbon downwind of Mexico City

X.-Y. Yu et al.

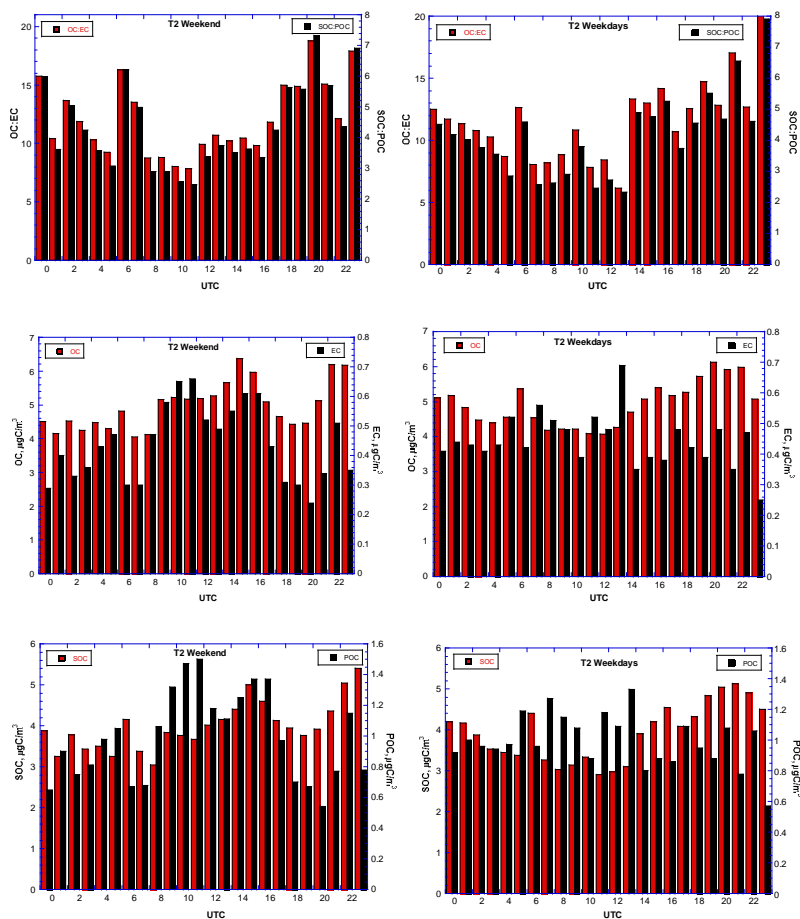


Fig. 10b. Average weekend (left column) and weekday (right column) patterns of OC/EC, SOC/POC, EC, OC, POC, and SOC at T2.

Title Page

Abstract

Introduction

Conclusions

References

Tables

Figures

◀

▶

◀

▶

Back

Close

Full Screen / Esc

Printer-friendly Version

Interactive Discussion

Primary and secondary organic carbon downwind of Mexico City

X.-Y. Yu et al.

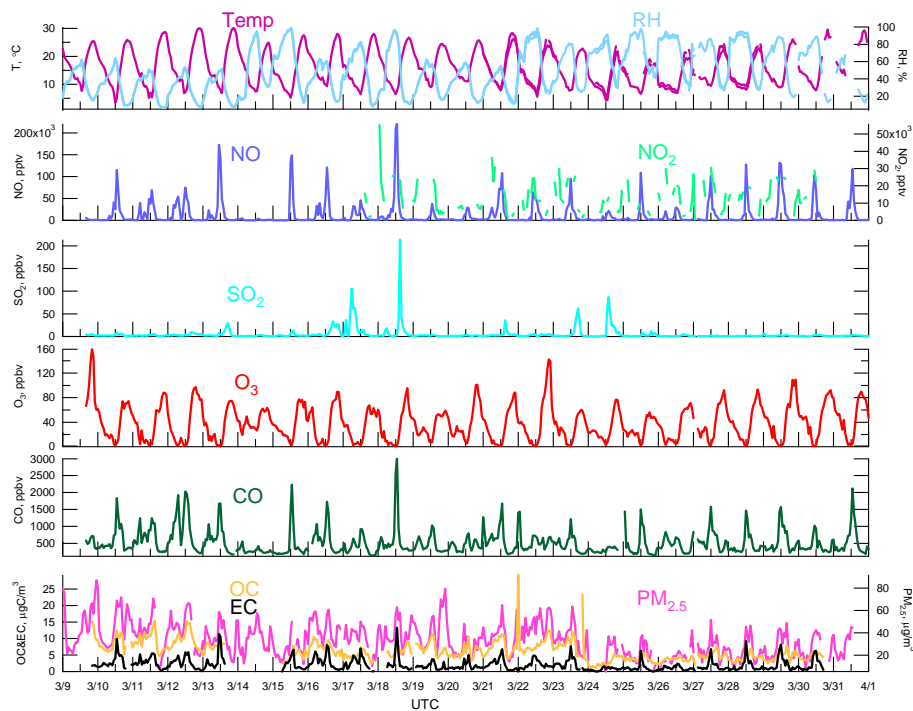
[Title Page](#)[Abstract](#)[Introduction](#)[Conclusions](#)[References](#)[Tables](#)[Figures](#)[◀](#)[▶](#)[◀](#)[▶](#)[Back](#)[Close](#)[Full Screen / Esc](#)[Printer-friendly Version](#)[Interactive Discussion](#)

Fig. 11. Time series of hourly OC, EC, $PM_{2.5}$, CO, O_3 , SO_2 , NO, NO_2 , temperature, and RH.

Primary and secondary organic carbon downwind of Mexico City

X.-Y. Yu et al.

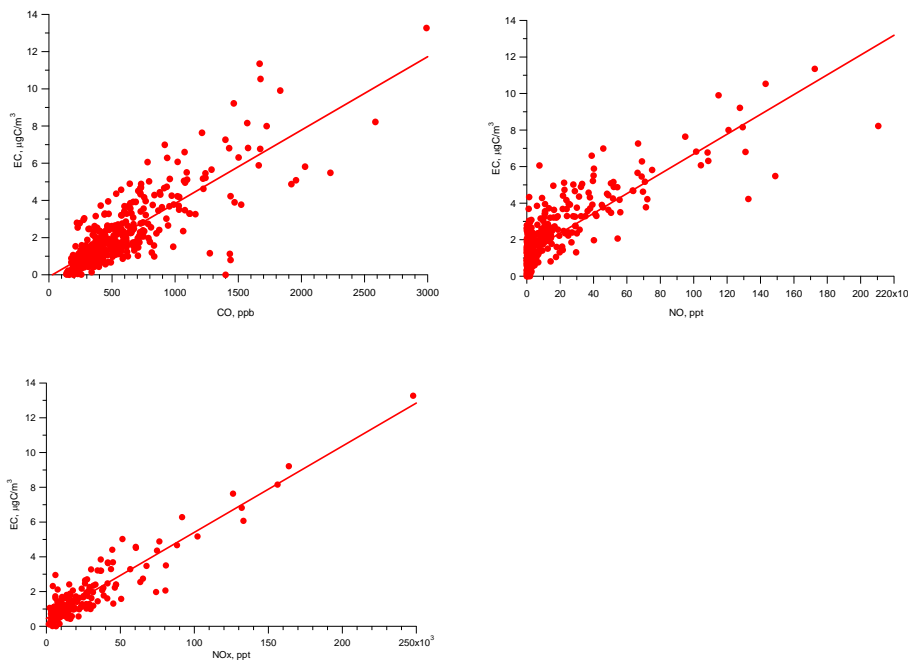


Fig. 12a. Scatter plots of EC vs. CO, EC vs. NO, EC vs. NO_x ($\text{NO}_x = \text{NO} + \text{NO}_2$). The solid lines are linear least-squares fits.

[Title Page](#)[Abstract](#)[Introduction](#)[Conclusions](#)[References](#)[Tables](#)[Figures](#)[◀](#)[▶](#)[◀](#)[▶](#)[Back](#)[Close](#)[Full Screen / Esc](#)[Printer-friendly Version](#)[Interactive Discussion](#)

**Primary and
secondary organic
carbon downwind of
Mexico City**X.-Y. Yu et al.

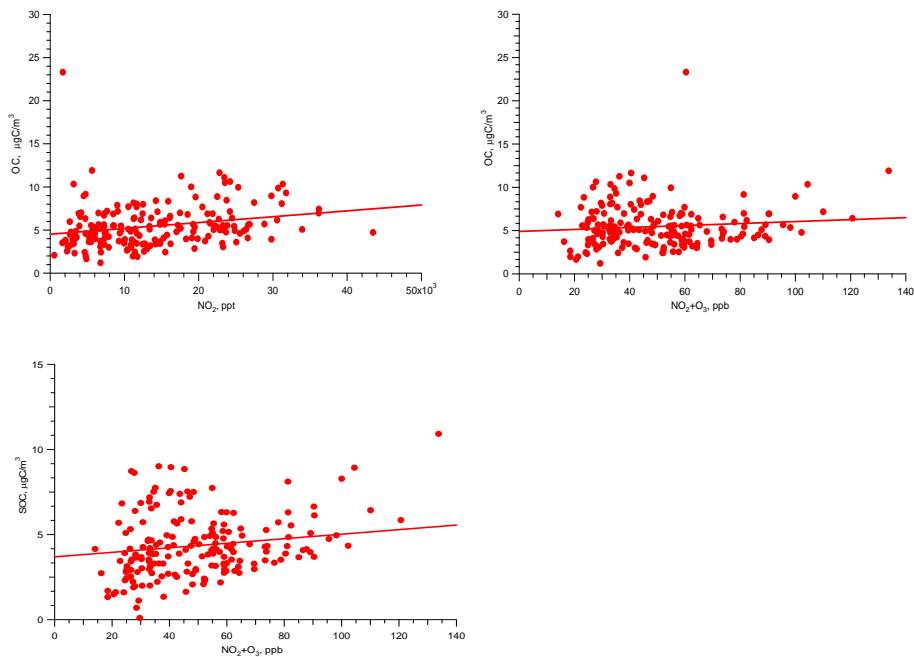


Fig. 12b. Scatter plots of OC vs. NO₂, OC vs. O_x (O_x=NO₂+O₃), and SOC vs. O_x (O_x=NO₂+O₃). The solid lines are linear least-squares fits.

[Title Page](#)[Abstract](#)[Introduction](#)[Conclusions](#)[References](#)[Tables](#)[Figures](#)[◀](#)[▶](#)[◀](#)[▶](#)[Back](#)[Close](#)[Full Screen / Esc](#)[Printer-friendly Version](#)[Interactive Discussion](#)

**Primary and
secondary organic
carbon downwind of
Mexico City**

X.-Y. Yu et al.

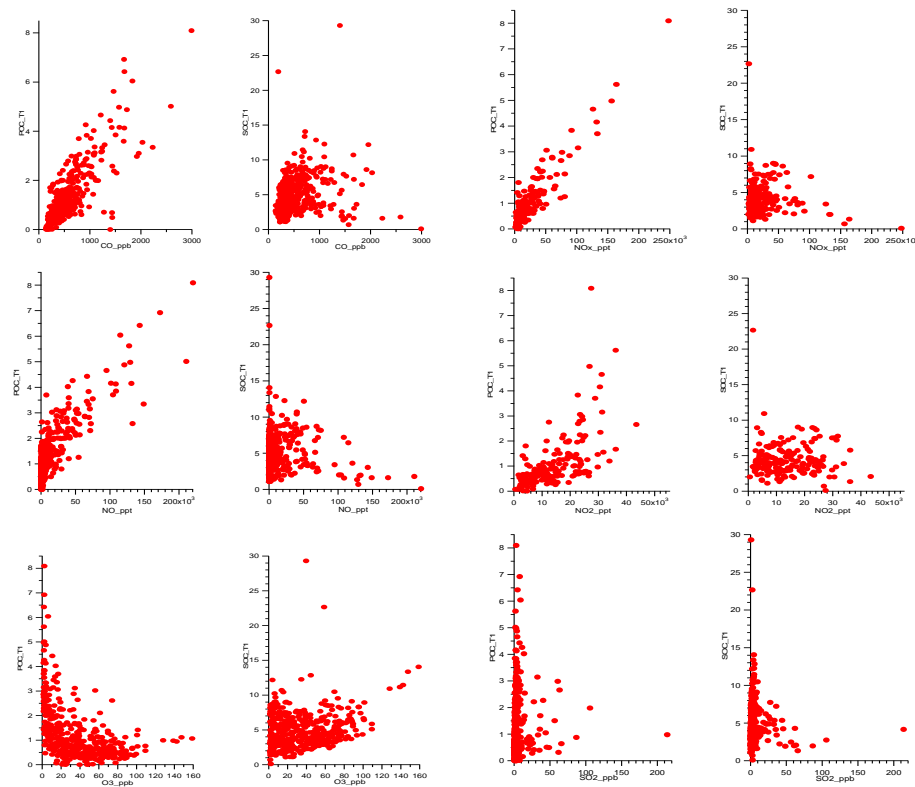


Fig. 13. Scatter plots of SOC and POC vs. CO, SOC and POC vs. NO_x, SOC and POC vs. NO, SOC and POC vs. NO₂, SOC and POC vs. O₃, and SOC and POC vs. SO₂, respectively at T1.

[Title Page](#)[Abstract](#)[Introduction](#)[Conclusions](#)[References](#)[Tables](#)[Figures](#)[◀](#)[▶](#)[◀](#)[▶](#)[Back](#)[Close](#)[Full Screen / Esc](#)[Printer-friendly Version](#)[Interactive Discussion](#)